NASA TECHNICAL NOTE

NASA TN D-7593

NASA TN D-7593

A METHOD OF AUTOMATICALLY STABILIZING HELICOPTER SLING LOADS

by Joseph Gera and Steve W. Farmer, Jr.

Langley Research Center
Hampton, Va. 23665

NATIONAL AERONAUTICS AND SPACE ADMINISTRATION • WASHINGTON, D. C. • JULY 1974

1. Report No. NASA TN D-7593	2. Government Accession No.	3. Recipient's Catalog No.
4. Title and Subtitle A METHOD OF AUTOMATICALLY STABILIZING HELICOPTER SLING LOADS		5. Report Date JULY 1974 6. Performing Organization Code
7. Author(s) Joseph Gera and Steve W. Farmer, Jr.		8. Performing Organization Report No. L-9371
9. Performing Organization Name and Address NASA Langley Research Center Hampton, Va. 23665		10. Work Unit No. 760-63-04-03 11. Contract or Grant No.
12. Sponsoring Agency Name and Address National Aeronautics and Space Administration Washington, D.C. 20546		13. Type of Report and Period Covered Technical Note 14. Sponsoring Agency Code

15. Supplementary Notes

16. Abstract

This report examines the effect of geometric and aerodynamic characteristics on the stability of the lateral degrees of freedom of a typical helicopter sling load. The feasibility of stabilizing the suspended load by controllable fins was also studied. Linear control theory was applied to the design of a simple control law that stabilized the load over a wide range of helicopter airspeeds.

17. Key Words (Suggested by Author(s))	18. Distribution Statement
Cargo helicopters Helicopter sling load Load stabilization	Unclassified – Unlimited STAR Category 02

19. Security Classif. (of this report)	20. Security Classif. (of this page)	21. No. of Pages	22. Price*
Unclassified	Unclassified	40	$3.25

*For sale by the National Technical Information Service, Springfield, Virginia 22151

A METHOD OF AUTOMATICALLY STABILIZING HELICOPTER SLING LOADS

By Joseph Gera and Steve W. Farmer, Jr.
Langley Research Center

SUMMARY

This report examines the lateral dynamic stability of a typical external helicopter load. A simple linear model representing the yawing and the pendulous oscillations of the sling-load system was used in the analysis. The effects of geometric and aerodynamic parameters, and of the helicopter airspeed, on the stability of the two modes of motion were studied. The feasibility of stabilizing external loads by means of controllable fins attached to the cargo was also examined. Linear optimal control theory was applied to the design of the control law for the stabilized sling. It was found that the use of constant feedback gains over the entire airspeed range considered was sufficient to stabilize a load such as an empty shipping container. A flexible computer program including real-time simulation of the motion with graphic display was developed during the course of this study.

INTRODUCTION

Experience with present day helicopters indicates that carrying loads externally is a more flexible mode of operation than internal loading and transportation of cargo. The development of the next-generation large flying-crane-type helicopters requires a critical evaluation of current external-load handling systems and techniques. One of the problems encountered in the external transportation of cargo is that cruise speeds with low-density high-drag suspended loads are restricted because of aerodynamic instability of these loads, particularly at the higher airspeeds. According to references 1 to 4, the problem of aerodynamic instability becomes apparent when at moderate forward speeds the various types of loads develop, first, yawing oscillations and, at still higher speeds, complete rotations. This motion is then coupled with lateral pendulous oscillations resulting in a difficult piloting task or a danger of load-helicopter contact. Except for near hovering flight, the longitudinal motions of the cargo do not cause handling difficulties; consequently, these motions will not be considered here.

Several experimental studies have been conducted to investigate the effect of multipoint suspension systems on sling-load instability. These suspension systems provide a

small amount of restoring moment in yaw, but may be insufficient to stabilize all types of suspended loads beyond some relatively low value of forward speed. A suggestion was made by William H. Phillips of the NASA Langley Research Center that a stabilized sling be used to overcome the aerodynamic instability of most slung loads. The sling would be equipped with a longitudinal spreader bar and actively operated aerodynamic controls or fins. The sling would be a permanent part of the helicopter's cargo handling system. An unloading operation, utilizing such a sling, is shown conceptually in figure 1. By properly sizing the controls or fins, it is expected that all types of loads could be stabilized with relatively small fin deflections over a wide range of airspeeds. One of the objectives of this investigation is to examine the lateral-directional stability of a typical sling load as a function of geometric characteristics and the aerodynamic derivatives of the load. Helicopter sling loads can be of all sizes and shapes so that generalizations are difficult to make. Field experience indicates, however, that aerodynamic instability occurs most frequently while carrying large low-density loads such as an empty shipping container. Accordingly, the lateral-directional stability of the linear model of the standard shipping container has been examined in some detail over a wide range of aerodynamic coefficients and operating conditions. Linear-optimal control theory was applied to the mathematical model to obtain feedback gains and to establish validity of the stabilized sling concept.

SYMBOLS

a_o section lift-curve slope, 2π rad^{-1}

a_f fin lift-curve slope, rad^{-1}

A fin aspect ratio

B control effectiveness matrix

C_D drag coefficient, D/qS

C_n yawing-moment coefficient, N/qSw

$C_{n_\beta} = \frac{\partial C_n}{\partial \beta}$, per rad

$C_{n_r} = \frac{2V_o}{w} \frac{\partial C_n}{\partial r}$, per rad

C_Y side-force coefficient, Y/qS

$C_{Y_\beta} = \frac{\partial C_Y}{\partial \beta}$, per rad

$C_{Y_r} = \frac{2V_o}{w} \frac{\partial C_Y}{\partial r}$, per rad

D drag force, N

F coefficient matrix of open-loop system

g gravitational acceleration, 9.81 m/sec^2

I identity matrix

I_Z moment of inertia about vertical axis, kg-m^2

$j = \sqrt{-1}$

k radius of gyration, $(I_Z/m)^{1/2}$, m

ℓ length of shipping container, 6.1 m

L cable length, m

m mass, kg

N yawing moment, N-m

$N_\beta = \frac{qSw}{I_Z} C_{n_\beta}$, per sec^2

$N_\psi = \frac{1}{I_Z} \frac{\partial N}{\partial \psi}$, per sec^2

$N_r = \frac{qSw^2}{2I_Z V_o} C_{n_r}$, per sec

$N_{\beta,1} = -\frac{qSw}{I_Z}\left(\frac{S_1}{S}\right)\left(\frac{\ell}{2w}\right) a_f$, per sec^2

$N_{\beta,2} = \frac{qSw}{I_Z}\left(\frac{S_2}{S}\right)\left(\frac{\ell}{2w}\right) a_f$, per sec^2

$N_{\delta,1} = \frac{qSw}{I_z}\left(\frac{S_1}{S}\right)\left(\frac{\ell}{2w}\right) a_f$, per sec^2

$N_{\delta,2} = \frac{qSw}{I_z}\left(\frac{S_2}{S}\right)\left(\frac{\ell}{2w}\right) a_f$, per sec^2

P	solution of matrix Riccati equation
q	dynamic pressure, $\frac{1}{2}\rho V_o^2$, N/m^2
Q	4 by 4 state-vector weighting matrix
r	yawing velocity, rad/sec
R	2 by 2 control-vector weighting matrix
S	reference area, 5.95 m^2
S_1	forward-fin area, 0.61 m^2
S_2	rear-fin area, 1.61 m^2
t	time, sec
u	control vector, $(\delta_1\ \delta_2)^T$
v	lateral velocity of load center of gravity, m/sec
V	total velocity, m/sec
V_o	towing speed, m/sec
x	state vector, $(y\ v\ \psi\ r)^T$
w	reference length (width), 2.4 m
y	lateral displacement of load center of gravity, m
Y	side force, N

$$Y_\beta = \frac{qS}{m} C_{Y_\beta}, \text{ m/sec}^2$$

$$Y_{\beta,1} = -\frac{qS}{m}\left(\frac{S_1}{S}\right) a_f, \text{ m/sec}^2$$

$$Y_{\beta,2} = -\frac{qS}{m}\left(\frac{S_2}{S}\right) a_f, \text{ m/sec}^2$$

$$Y_y = \frac{g}{L}, \text{ per sec}^2$$

$$Y_r = \frac{qSw}{2mV_o} C_{Y_r}, \text{ m/sec}$$

$$Y_{\delta,1} = \frac{qS}{m}\left(\frac{S_1}{S}\right) a_f, \text{ m/sec}^2$$

$$Y_{\delta,2} = \frac{qS}{m}\left(\frac{S_2}{S}\right) a_f, \text{ m/sec}^2$$

α sensitivity parameter

β angle of sideslip, $\frac{v}{V_o} - \psi$, rad

δ_1, δ_2 control fin deflections, rad

ϵ_1, ϵ_2 lateral cable angles, rad

λ_i ith characteristics value of F

λ_p characteristic value associated with pendulous mode

λ_y characteristic value associated with yaw mode

ρ atmospheric density, kg/m^3

ψ angle of yaw, rad

ω_p, ω_y angular frequency of pendulum and yaw mode, respectively, rad/sec

The symbols $\frac{d}{dt}$ or ($\dot{}$) denote time derivatives; the superscript T denotes matrix transpose.

ANALYSIS

Stability Investigation

The full nonlinear equations of motion of a helicopter and a sling load with a two-point or bifilar suspension have been derived in reference 5. Mathematical treatment of these equations is possible only after linearization. In reference 5 aerodynamic forces and moments acting on the load were neglected in the process of linearization. For hovering flight this is a valid assumption; for the case under consideration the effects of aerodynamic forces and moments are as important as those transmitted by the cables and were added for this analysis. It will be assumed that the motion of the load has both a yawing and a pendulous component in the lateral direction. The helicopter is assumed to be in a level, nonaccelerating flight at all times. Longitudinal deflections of the cables due to drag on the load and the cables themselves are neglected. These assumptions correspond to the load being suspended from the top wall in a wind-tunnel test section with the tunnel speed being constant. This condition is similar to the test conditions which are described in reference 6 in connection with an experimental investigation of external sling-load instabilities. Small oscillations will be assumed and the effect of the stabilizing fins will be included separately. The notation used is shown in sketch a.

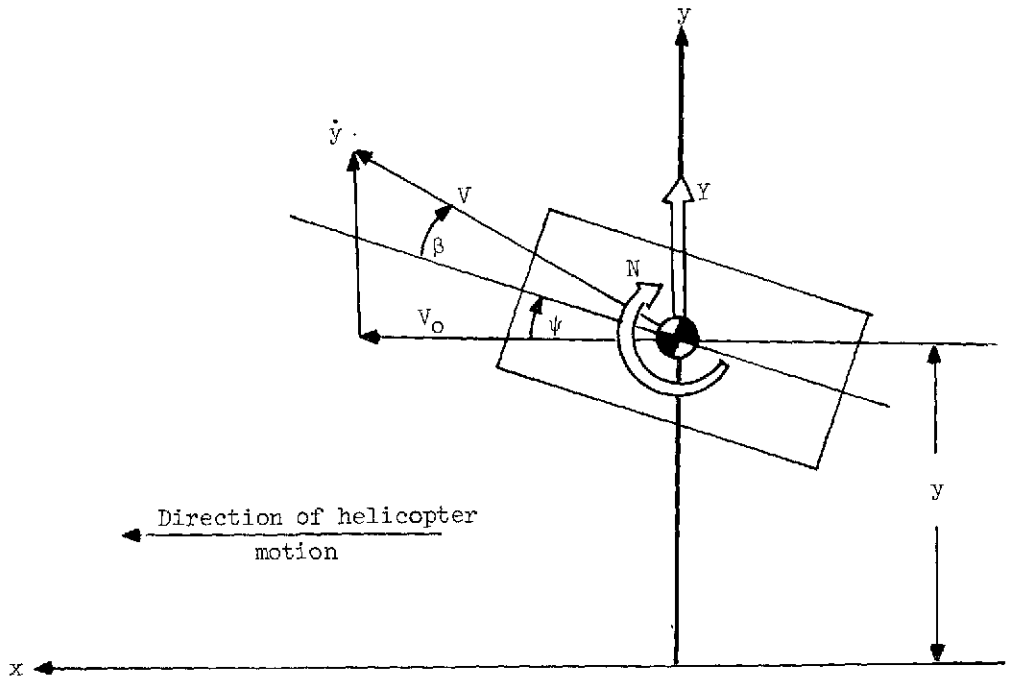

Sketch a

The linearized lateral equations of motion of a suspended body are given in reference 7. After minor modifications these equations also describe the motion of a helicopter sling load as shown by

$$m\ddot{y} = \frac{\partial Y}{\partial \dot{y}}\dot{y} + \frac{\partial Y}{\partial \dot{\psi}}\dot{\psi} + \frac{\partial Y}{\partial y}y + \frac{\partial Y}{\partial \beta}\beta$$

$$I_z\ddot{\psi} = \frac{\partial N}{\partial \dot{\psi}}\dot{\psi} + \frac{\partial N}{\partial \beta}\beta + \frac{\partial N}{\partial \psi}\psi$$

along with the kinematic relationship

$$\dot{y} = (\beta + \psi)V_o$$

In the following discussion, let $\dot{y} = v$ and $\dot{\psi} = r$. Further, define the stability derivatives as

$$Y_\beta = \frac{1}{m}\frac{\partial Y}{\partial \beta}$$

$$N_\beta = \frac{1}{m}\frac{\partial N}{\partial \beta}$$

and the other derivatives similarly. The above equations then become

$$\frac{d}{dt}\begin{bmatrix} y \\ v \\ \psi \\ r \end{bmatrix} = \begin{bmatrix} 0 & 1 & 0 & 0 \\ Y_y & \frac{1}{V_o}Y_\beta + Y_{\dot{y}} & -Y_\beta & Y_r \\ 0 & 0 & 0 & 1 \\ 0 & \frac{1}{V_o}N_\beta & N_\psi - N_\beta & N_r \end{bmatrix}\begin{bmatrix} y \\ v \\ \psi \\ r \end{bmatrix} \tag{1}$$

All derivatives are due to aerodynamic forces and moments except Y_y and N_ψ. These two derivatives can be evaluated with the aid of sketch b.

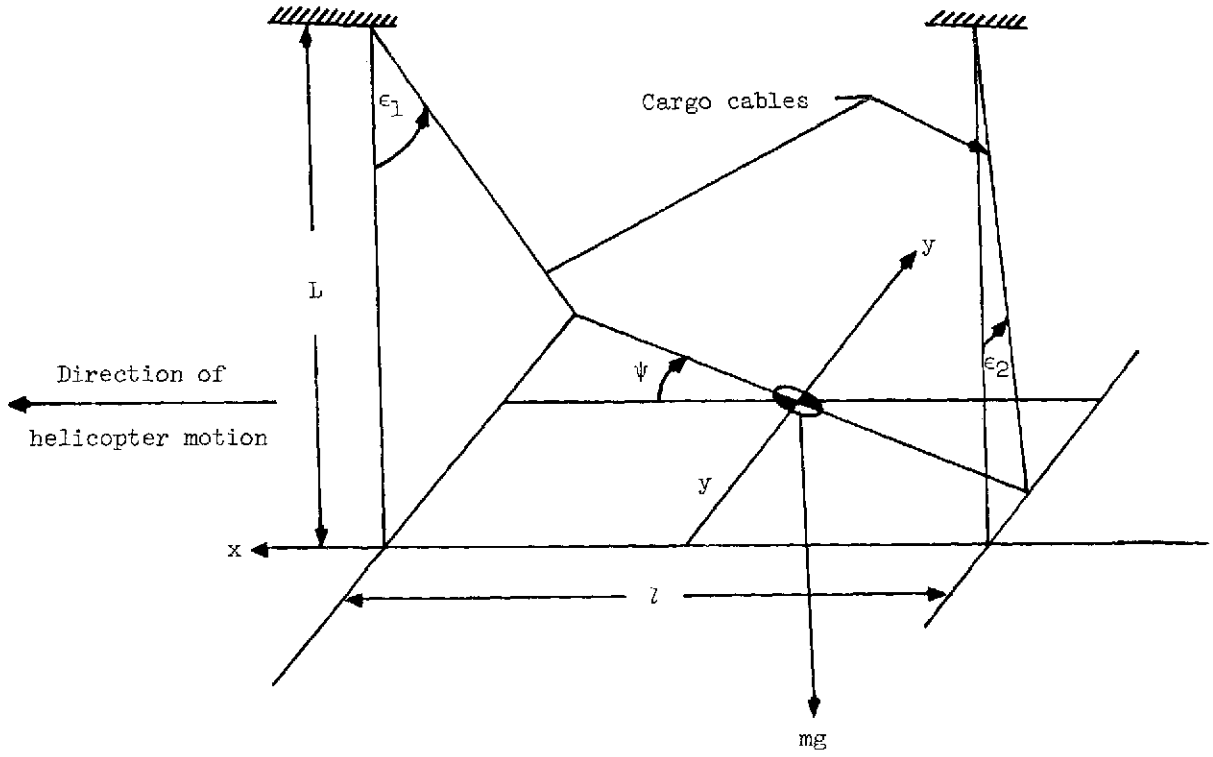

Sketch b

The gravitational portion of restoring force acting at the center of gravity as shown is

$$Y = \frac{-mgy}{L}$$

so that

$$\frac{1}{m}\frac{\partial Y}{\partial y} = Y_y = -\frac{g}{L}$$

The restoring moment due to the bifilar suspension can be expressed as

$$N = -\frac{\ell^2 mg}{4L}\psi$$

from which

$$\frac{1}{I_z}\frac{\partial N}{\partial \psi} = N_\psi = -\frac{\ell^2 g}{4k^2 L}$$

where k is the radius of gyration of the suspended load.

The derivative $Y_{\dot{y}}$ is due to the component of aerodynamic drag of the load acting in the lateral or y-direction. The magnitude of this component for small oscillations is $-D(\beta + \psi)$. Since

$$D(\beta + \psi) = \frac{D\dot{y}}{V_o}$$

it follows that

$$\frac{1}{m}\frac{\partial Y}{\partial \dot{y}} = Y_{\dot{y}} = \frac{-D}{mV_o}$$

The definitions of the remaining derivatives follow those used in conventional-airplane stability analysis and are given in the list of symbols.

The five nondimensional aerodynamic derivatives, C_D, C_{Y_β}, C_{Y_r}, C_{n_β}, and C_{n_r}, associated with a boxlike shape such as the standard shipping container are not precisely known. Wind-tunnel measurements made on small models are subject to scale errors, while theoretical predictions do not take into account large regions of separated flow. Also, there are indications that in the case of strictly nonaerodynamic shapes the validity of the linear air reaction assumption may be open to question. The numerical values of the above derivatives were selectively chosen from several sources, none of which claimed any degree of precision. Therefore, values of some of the derivatives were adjusted slightly until time histories of the motion variables agreed at least qualitatively with flight test experience with container-type cargo. Such flight tests are described in some detail in reference 3. After some experimentation, a set of aerodynamic derivatives were selected for the remainder of the analysis. The set which reproduced qualitatively the motion of the slung cargo is given in table I.

The mathematical model exhibited two kinds of lateral oscillations: a pendulum-like motion and a yawing motion which usually had a higher frequency. Also, the yawing motion had a greater tendency to become unstable as the towing velocity increased.

Figure 2 shows the individual effect of changing the cable length, load mass radius of gyration, and atmospheric density on the characteristic values associated with the pendulum-like motion at various forward velocities. At low velocities the frequency of the motion approaches that of the simple mathematical pendulum given by $\sqrt{g/L}$ rad/sec. At the highest velocities, typically at 61.3 and 77.3 m/sec, the pendulous motion became a divergence and a subsidence. The real characteristic roots associated with these motions are not shown on the graph. The effects of cable length, load mass, and atmospheric density on the pendulous motion are what might be expected intuitively.

From figure 2(c) it is interesting to note that increasing the radius of gyration had a definite effect on the pendulous motion; at higher velocities, damping is reduced. Intuitively, one would expect no effect of the radius of gyration on the pendulous motion. The decreased damping was caused by the close coupling between the pendulous and yawing oscillations. Thus, in the case of the slung helicopter cargo it is not possible to consider either mode separately.

The behavior of the characteristic roots associated with the yawing motion is shown in figure 3. At low velocities the frequency of the yawing oscillations is close to the natural frequency of a simple bifilar pendulum. The frequency in terms of the parameters used herein is given by

$$\omega_y = \frac{l}{2k}\sqrt{\frac{g}{L}}$$

At higher velocities the restoring moment due to the bifilar suspension is overcome by the yawing moment due to sideslip. Examination of the effect of load mass in figure 3(b) reveals that in the medium velocity range increasing the mass has a stabilizing influence on the yawing motion. Increasing the radius of gyration results in increased damping at the higher airspeeds according to figure 3(c). At low airspeeds, however, the increased radius of gyration has the opposite effect. The atmospheric density has only a weak effect on either the pendulous or yawing oscillation.

On the basis of the results presented in figures 2 and 3, it can be stated that the cargo configuration which would have the greatest tendency to exhibit unstable oscillations as the airspeed is increased is the low density cargo. Field experience, reported in references 2 and 3, confirms this result. Consequently, the low-density cargo with medium cable length and atmospheric density at sea level was selected for an examination of the effect of small changes in the aerodynamic derivatives at low (25.7 m/sec) and medium (51.5 m/sec) forward velocities. This was accomplished by applying the procedure described in reference 8. The procedure consisted of computing the complex number

$$\frac{\partial \lambda_i}{\partial \alpha} = \frac{\text{trace of } \left\{\left[\text{adj}(F - \lambda_i I)\right] \frac{\partial F}{\partial \alpha}\right\}}{\text{trace of } \left\{\text{adj}(F - \lambda_i I)\right\}}$$

where F is the coefficient matrix in equation (1), λ_i is the ith distinct characteristic value of F, and α is the parameter whose effect on the real and imaginary part of λ_i is sought. The computation of $\frac{\partial \lambda_i}{\partial \alpha}$ is straightforward, but tedious, for even low-order dynamic systems. In table II the results of the computation are summarized; and the relative importance of the five aerodynamic derivatives are shown. The numerical entries in the table refer only to the single root located in the upper half plane in all

cases, rather than to each of the conjugate pair associated with an oscillatory motion. The derivative C_{n_β} is seen to have the greatest influence on the character of the motion. Furthermore, it is through this derivative that the two modes are closely coupled. It is interesting to note from the table that the times to damp to half amplitude of the two modes are influenced by C_{n_β} and C_{Y_r} to the same extent, but in the opposite sense as far as the stability of the two modes are concerned. In general, experience with the sensitivity coefficients indicates that they reflect the true effect of the parameter change only in a small region about the characteristic value, λ_i in question; gross changes in α may even result in a location of λ_i in the complex plane opposite to the direction indicated by the sensitivity coefficient $\frac{\partial \lambda_i}{\partial \alpha}$.

Load Stabilization

In the preceding section it was shown that the assumed mathematical model can become unstable at forward velocities exceeding about 50 m/sec. Even if allowances are made for the additional drag due to the load, helicopters in use today are capable of exceeding 50 m/sec in forward flight. Automatic stabilization of slung loads would therefore allow a better utilization of crane-type helicopters by speeding up such repetitive operations as the unloading or loading of containerized shipping cargo when it must be carried over some distance. Stabilization of sling loads can be accomplished through the automatic flight control system of the helicopter, if it is so equipped, or by the use of external stabilizing devices such as controllable fins. The latter method appears simpler in principle and is effective in the flight regime where it is needed most, that is, in high-speed forward flight. Such a load-stabilizing device would be a permanent part of the load-carrying system of the helicopter using controllable fins positioned by electromechanical servoactuators with the necessary power being transmitted through the load-carrying cables. The fin position commands would be continuously computed, based on the lateral position and velocity of the cargo relative to the helicopter. The objective of the commands would be to keep the cargo at the constant position at zero lateral velocity relative to the helicopter. Thus, the problem of stabilizing the load can be regarded as the classical regulator problem.

Sketch c shows the configuration chosen for the controllable fins. It consists of a spreader bar which would be attached rigidly to the cargo. Positive deflections of the front and rear fins are also shown on the sketch.

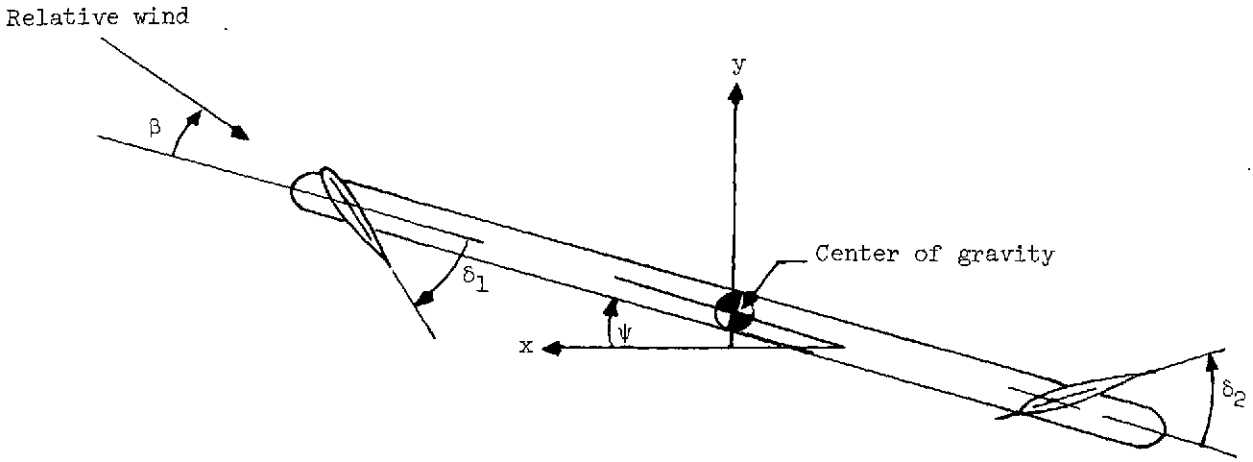

Sketch c

Note that the fin deflections are defined in such a way that at zero sideslip angle positive δ_1 and δ_2 result in positive yawing moment about the center of gravity. It will be assumed that the forces on the front and rear fin contribute to the total side force and yawing moment of the load, but that the mass of the spreader bar and fin assembly is negligible relative to the mass of the load. The fin lift-curve slope a_f is approximated by the expression

$$a_f = \frac{a_o}{1 + \frac{a_o}{\pi A}}$$

where a_o is the section lift-curve slope for infinite aspect ratio and A is the aspect ratio of the fin. In the remaining discussion, an aspect ratio of unity and a fin section lift-curve slope of 2π per radians will be assumed.

In the linear equations of motion the addition of the controllable fins is accounted for in the following way:

$$\frac{d}{dt}\begin{bmatrix} y \\ v \\ \psi \\ r \end{bmatrix} = \begin{bmatrix} 0 & 1 & 0 & 0 \\ Y_y & \frac{1}{V_o}\left(Y_\beta + Y_{\beta,1} + Y_{\beta,2}\right) + Y_{\dot{y}} & -Y_\beta - Y_{\beta,1} - Y_{\beta,2} & Y_r \\ 0 & 0 & 0 & 1 \\ 0 & \frac{1}{V_o}\left(N_\beta + N_{\beta,1} + N_{\beta,2}\right) & N_\psi - \left(N_\beta + N_{\beta,1} + N_{\beta,2}\right) & N_r \end{bmatrix} \begin{bmatrix} y \\ v \\ \psi \\ r \end{bmatrix} + \begin{bmatrix} 0 & 0 \\ Y_{\delta,1} & Y_{\delta,2} \\ 0 & 0 \\ N_{\delta,1} & N_{\delta,2} \end{bmatrix} \begin{bmatrix} \delta_1 \\ \delta_2 \end{bmatrix}$$

or in vector-matrix form

$$\dot{x} = Fx + Bu$$

where the additional entries in the 4 by 4 matrix F and the elements of B are defined in the list of symbols.

The addition of the controllable fins obviously alters the aerodynamic characteristics of the shipping container even if the fins are assumed to be in a stationary position alined with the longitudinal axis of the container. Because of the small size of the fins relative to the overall dimension of the shipping container and the uncertainty of the aerodynamic data, it was assumed in the present analysis that the fins do not contribute to the damping derivatives C_{Y_r} and C_{n_r} and their effect on the drag coefficient C_D is negligible. Figure 4 shows the effect of attaching a front and rear fin to the shipping container when both fins are locked at zero deflection. The graph indicates slight changes in the characteristic values but the overall characteristics of the motion are unaltered.

The objective of bringing the cargo from any initial displacement or velocity into the plane of symmetry of the towing helicopter in the shortest time by as small control deflections as possible is equivalent to the minimization of the functional J defined as follows:

$$J = \int_0^\infty \left[u^T(t)\, Ru(t) + x^T(t)\, Qx(t)\right] dt$$

where R and Q are any symmetric, positive definite and nonnegative definite matrices, respectively. Under these hypotheses an optimal feedback control law, $u^*(t)$, exists and is given by

$$u^*(t) = -R^{-1}B^TPx(t) \tag{2}$$

where the matrix P satisfies the algebraic matrix Riccati equation

$$PF + F^TP - PBR^{-1}B^TP + Q = 0 \tag{3}$$

For a detailed treatment of linear systems optimization the reader is referred to one of the numerous textbooks on the subject (e.g., ref. 9). Application of the theory to the present problem provides for two significant advantages in addition to the immediate result of the linear control law expressed by equation (2). These are as follows: first, a sufficient condition that the closed-loop system will have no unstable characteristic values as long as the matrix Q be chosen as a diagonal matrix with positive real elements, and, second, the fin deflections δ_1 and δ_2 can be kept within reasonable bounds by means of increasing or decreasing their relative weights in the performance index through appropriate choice of R. Thus, the problem of designing the feedback control law which guarantees stability

is essentially reduced to solving the algebraic equation (2) for the matrix P. This was accomplished by an iterative technique described in reference 10.

The optimal control law is relatively simple; it is a linear combination of the elements of the state vector $x(t)$ at any instant. In order for it to be of any engineering use, however, these elements must be measurable. It turns out that for small displacements the state vector can be easily computed by measuring the cable angles ϵ_1 and ϵ_2, as defined previously, and the rate at which these angles change. The formulas that are involved are as follows:

$$y = \frac{L}{2}\epsilon_1 + \frac{L}{2}\epsilon_2$$

$$\psi = \frac{L}{l}(\epsilon_1 - \epsilon_2)$$

Then, by taking the time derivatives of the two expressions,

$$\begin{bmatrix} y \\ v \\ \psi \\ r \end{bmatrix} = \begin{bmatrix} L/2 & 0 & L/2 & 0 \\ 0 & L/2 & 0 & L/2 \\ L/l & 0 & -L/l & 0 \\ 0 & L/l & 0 & -L/l \end{bmatrix} \begin{bmatrix} \epsilon_1 \\ \dot{\epsilon}_1 \\ \epsilon_2 \\ \dot{\epsilon}_2 \end{bmatrix}$$

In addition to the cable angles ϵ_1 and ϵ_2 and their time derivatives, the cable length must be known or measurable; measurement of the cable length should present no unusual problems. Thus, the complete construction of the state vector $x = (y\ v\ \psi\ r)^T$ appears feasible. The remaining obstacle associated with the application of the optimal control theory is that the elements of the matrix F change with forward velocity and a new set of optimal gains must be computed for significant changes of the matrix F. Alternately, one can hope for determining a single set of gains which will result in desirable properties of the closed-loop system over the entire speed range. In this investigation the latter approach was successfully used. The success of this approach was brought about by extensive use of a high-speed computer with on-line recording and display devices. Several sets of gains were found which stabilized the load at any speed, and over the entire range of aerodynamic coefficient and geometric parameters considered in the stability investigation. Since the computing procedure is believed to be unique, it is described in some detail in the appendix.

Results With Controlled Fins

The computer program described in the appendix can be used as a design tool. Feedback gains, which were not only optimal for a particular set of geometric and aerodynamic configurations but also stabilized the system for a wide range of conditions, were found very quickly and efficiently. An example of these computations is described for the light cargo with small radius of gyration and medium cable length at a towing speed of 51.5 m/sec. This configuration was markedly unstable in yaw at this speed and was one of the least stable configurations examined. Minimization of the functional J, penalizing nonzero values of both the control and state, namely,

$$J = \int_0^\infty \left[u^T(t)\, Ru(t) + x^T(t)\, Qx(t)\right] dt$$

for a choice of the matrices R and Q, where

$$R = \begin{bmatrix} 500 & 0 \\ 0 & 500 \end{bmatrix} \qquad Q = \begin{bmatrix} 1 & 0 & 0 & 0 \\ 0 & 1 & 0 & 0 \\ 0 & 0 & 1 & 0 \\ 0 & 0 & 0 & 1 \end{bmatrix}$$

resulted in the following feedback control law

$$u^*(t) = \begin{bmatrix} +0.0019 & -0.0398 & -2.566 & -3.068 \\ +0.0074 & -0.0196 & -2.048 & -2.838 \end{bmatrix} x(t) \qquad (4)$$

It should be noted that the feedback control law specifies different gains for the two control fins. The difference is particularly noticeable for the lateral displacement. This result arises from the fact that it is more effective to translate the cargo by yawing and using the resulting side force for lateral translation than by using the control fins as direct-force devices.

Time histories of the closed-loop system variables are shown in figure 5. For comparison, time histories are also presented using the same feedback gain matrix at the airspeeds 15.4 m/sec and 77.3 m/sec. The figure shows that the fin deflections are moderate with maximum rates well within the capabilities of current servoactuators. The overall stability characteristics are shown on figure 6 where the characteristic values associated with the yawing and pendulous motion are shown for various values of towing

speed. In contrast to the open-loop system, the closed-loop configuration is seen to be well damped in yaw and stable at all towing speeds. The level of stability is actually increasing with towing speed.

The feedback gains of the previous example were found to stabilize the system over the entire range of geometric parameters and speed range. Also, the closed-loop configuration was found to be insensitive to moderate changes in the aerodynamic derivatives. No detailed investigation was performed on the effect of varying the aerodynamic derivatives in a systematic fashion. This would have involved generation of large amounts of data based on a set of assumed aerodynamic derivatives; it was felt more desirable to make the computer program as flexible as possible for future use with better known aerodynamic data.

The linear control law expressed in equation (4) was used to simulate failure of the front-fin or rear-fin servoactuators. In this simulation it was assumed that as soon as servo failure is detected, the actuator would be disengaged so that the fin can aline itself with the relative wind. In this position, the net contribution of the faulty fin to the overall lateral force and moment acting on the cargo would be negligible. This type of failure of the front fin, for example, can be simulated by setting the coefficients $Y_{\beta,1}$, $N_{\beta,1}$, $Y_{\delta,1}$, and $N_{\delta,1}$ equal to zero.

Figure 7 shows the position of the characteristic values in the complex plane with either the front or rear fin failed for the configuration used in the previous figure. The effect of servo failure is negligible on the pendulum mode of the motion. Although the effect on the yaw mode is noticeable, it is significant that the motion remained stable throughout the whole range of towing speeds.

CONCLUDING REMARKS

External helicopter loads of the rectangular-box type suspended from long cargo slings are usually unstable aerodynamically beyond some value of airspeed. The use of a stabilized sling has been suggested to avoid operational problems due to this instability.

According to the available documented experience, load instability occurs, even at moderate speeds, while carrying large low-density objects such as an empty shipping container. Most frequently, the instability is a divergent yawing oscillation.

A linear mathematical model of the externally carried helicopter load was studied. Only the lateral modes of motion were considered with and without the stabilized sling. It was also assumed that the helicopter motion is unaffected by the sling load. The following conclusions were drawn from the study.

The dynamic stability characteristics of the suspended helicopter cargo were reproduced, at least qualitatively, using realistic combinations of geometric and aerodynamic parameters in the linear model.

Linear optimal control theory was applied to the problem of stabilization, and it proved to be effective in the design of feedback control laws which stabilized the motion over the whole range of configurations with the use of constant feedback gains. The variables used in the feedback law can be reconstructed by measuring the lateral angular deflections and velocities of the suspension cables. Implementation of the feedback control law requires moderate deflections and rates from the controllable fins. Use of a single fin for stabilization also appears feasible.

A computer program developed for the present investigation proved to be an effective design tool. Its flexibility would allow meeting design criteria other than just stabilizing the suspended cargo.

Langley Research Center,
National Aeronautics and Space Administration,
Hampton, Va., April 15, 1974.

APPENDIX

REAL-TIME DIGITAL COMPUTER PROGRAM FOR HELICOPTER SLING LOADS STUDY

A real-time digital computer program was developed for the math model of this study. The program was written in Fortran IV language, occupying 55 000 octal locations of memory, and run on the Control Data series 6000 digital computer complex. Figure 8 is a functional block flow diagram of the computer program. All constants, initial conditions, aerodynamic derivatives, and integration parameters are defined in the first two blocks. An optimization loop takes the initial conditions and constants and calculates the feedback gains. Once the feedback gains have been calculated, this section of the computer program is no longer cycled through. The program then gives the choice of either selecting an open-loop or a closed-loop system to be run for data gathering.

The real-time solution of a set of differential equations is a discrete or step process. The time it takes for each step is called frame time. The computer reads inputs at the beginning of each frame time and the outputs are transmitted at the end of each frame time. During each frame time, the computer does all calculations necessary to advance the equations of motion one integration step. The simulation program of this report operated at 32 frames per second, so that the frame time was 30.125 milliseconds.

The integration scheme used was a second-order Runge-Kutta. A fourth-order Runge-Kutta integration scheme was tried for a check of the RK-2 scheme with no noticeable difference in the computed response. As a check on the size of the frame time used, the program was run at 64 frames per second and 128 frames per second to insure that the computed responses of the dynamic system were not being degraded. No changes in the computed responses of the dynamic system were detected. The real-time program was also checked with an independent batch program to insure coding correctness. The printouts from the real-time-simulation (RTS) program and the independent check program of the eigenvalues and state variables compared exactly to seven or eight decimal places.

This program was operated in real time instead of batch processing because this allows control of and interaction with the computer program by the researcher at the real-time control station. Figure 9 shows a typical program control station with all components that are available for use. Using the function sense switches and discrete inputs on the control panel, the researcher can make a data run, change a program parameter or initial condition, and then immediately make another data run. For the problem of this report, data runs were made by varying initial conditions on several variables, the aerodynamic coefficients, and geometric constants.

The real-time system also provides the capability of displaying the program on the cathode-ray tube (CRT). Through the use of a keyboard at the CRT console, programing errors can be corrected and/or additions to the program can be made while it is still resident in the computer. The CRT was also used to present a visual display representing the moving shipping container. This display was observed to determine whether the data run was satisfactory. Thus the real-time facility gives the researcher the ability to make data runs while observing the results on a time-history recorder and/or a CRT display. (For a more complete description of the real-time facility, see ref. 11.) In this manner data runs were made during a 2-hour period on the RTS facility that would have taken several days using batch processing.

REFERENCES

1. Liv, David T.: In-Flight Stabilization of Externally Slung Helicopter Loads. USAAMRDL Tech. Rep. 73-5, U.S. Army, May 1973.

2. Hutto, A. J.: Qualitative Commentary on Tandem Helicopter External Cargo Sling Operation. Proceedings of the Twenty-Second Annual National Forum, Amer. Helicopter Soc., May 1966, pp. 185-192.

3. Hutto, A. J.: Qualitative Report on Flight Test of a Two-Point External Load Suspension System. Preprint No. 473, Amer. Helicopter Soc., June 1970.

4. Szustak, Leonard S.; and Jenney, David S.: Control of Large Crane Helicopters. J. Amer. Helicopter Soc., vol. 16, no. 3, July 1971, pp. 11-22.

5. Abzug, M. J.: Dynamics and Control of Helicopters With Two-Cable Sling Loads. AIAA Paper No. 70-929, July 1970.

6. Gabel, Richard; and Wilson, Gregory J.: Test Approaches to External Sling Load Instabilities. J. Amer. Helicopter Soc., vol. 13, no. 3, July 1968, pp. 44-55.

7. Phillips, W. H.: Stability of a Body Stabilized by Fins and Suspended From an Airplane. NACA WR L-28, 1944. (Formerly NACA ARR L4D18.)

8. Reddy, D. C.: Evaluation of the Sensitivity Coefficient of an Eigenvalue. IEEE Trans. Automatic Cont., vol. AC-12, no. 6, Dec. 1967, p. 792.

9. Anderson, Brian D. O.; and Moore, John B.: Linear Optimal Control. Prentice-Hall, Inc., c.1971.

10. Kleinman, David L.: On an Iterative Technique for Riccati Equation Computations. IEEE Trans. Automatic Contr., vol. AC-13, no. 1, Feb. 1968, pp. 114-115.

11. Grove, Randall D.; and Mayhew, Stanley C.: A Real-Time Digital Program for Estimating Aircraft Stability and Control Parameters From Flight Test Data by Using the Maximum Liklihood Method. NASA TM X-2788, 1973.

TABLE I.- ASSUMED NOMINAL CONFIGURATION AND AERODYNAMIC CHARACTERISTICS OF SHIPPING CONTAINER

Mass, kg	2266
Radius of gyration, m	1.9
Atmospheric density, kg/m^3	1.23
Cable length, m	30.5
C_D	1.1
C_{Y_β}, rad^{-1}	-1.5
C_{Y_r}, rad^{-1}	2.0
C_{n_β}, rad^{-1}	-0.25
C_{n_r}, rad^{-1}	-1.25

TABLE II.- EFFECT OF AERODYNAMIC DERIVATIVES ON CHARACTERISTIC VALUES

α	Pendulous mode, $\frac{\partial \lambda_p}{\partial \alpha}$, for –		Yawing mode, $\frac{\partial \lambda_y}{\partial \alpha}$, for –	
	V_o = 15.4 m/sec	V_o = 51.5 m/sec	V_o = 15.4 m/sec	V_o = 51.5 m/sec
C_{n_β}	0.01215 + 0.002347j	-0.17637 + 4.56045j	-0.01215 + 0.1462j	[a] 0.17637 + 0.67729j
C_{Y_β}	0.014173 + 0.00107j	0.06915 + 0.08087j	-0.00175 - 0.00032j	[a] -0.02775 - 0.03839j
C_D	0.01238 + 0.00085j	0.01308 + 0.00278j	0.00004 - 0.00013j	[a] 0.02833 + 0.01102j
C_{n_r}	0.00002 - 0.00007j	0.02023 + 0.02107j	0.01026 + 0.00022j	[a] 0.01404 - 0.00839j
C_{Y_r}	0.00001 - 0.00008j	0.00068 + 0.00004j	-0.00001 + 0.00012j	[a] -0.00068 + 0.00087j

[a] Unstable mode.

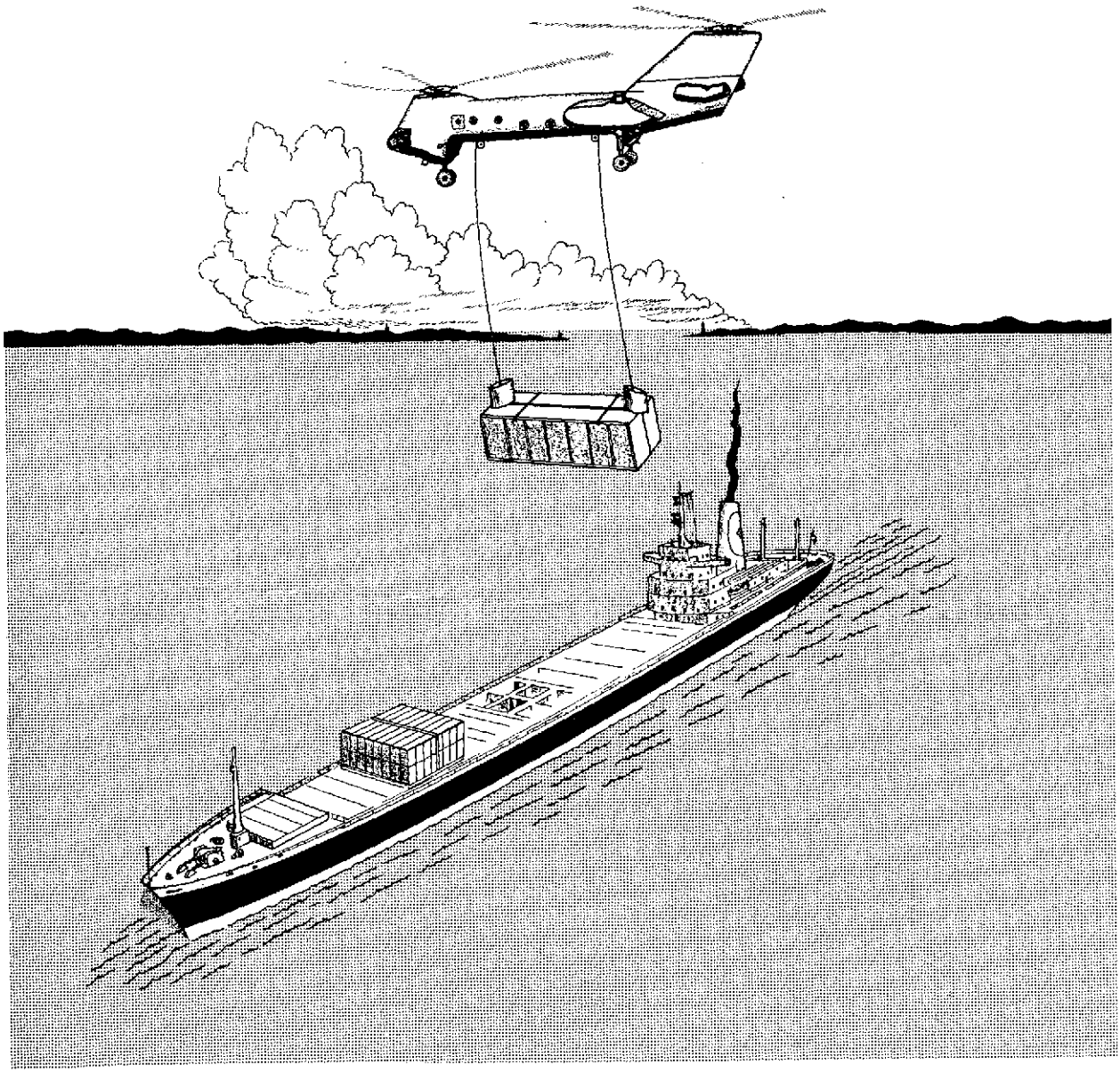

Figure 1.- An artist's rendition of using the stabilized sling.

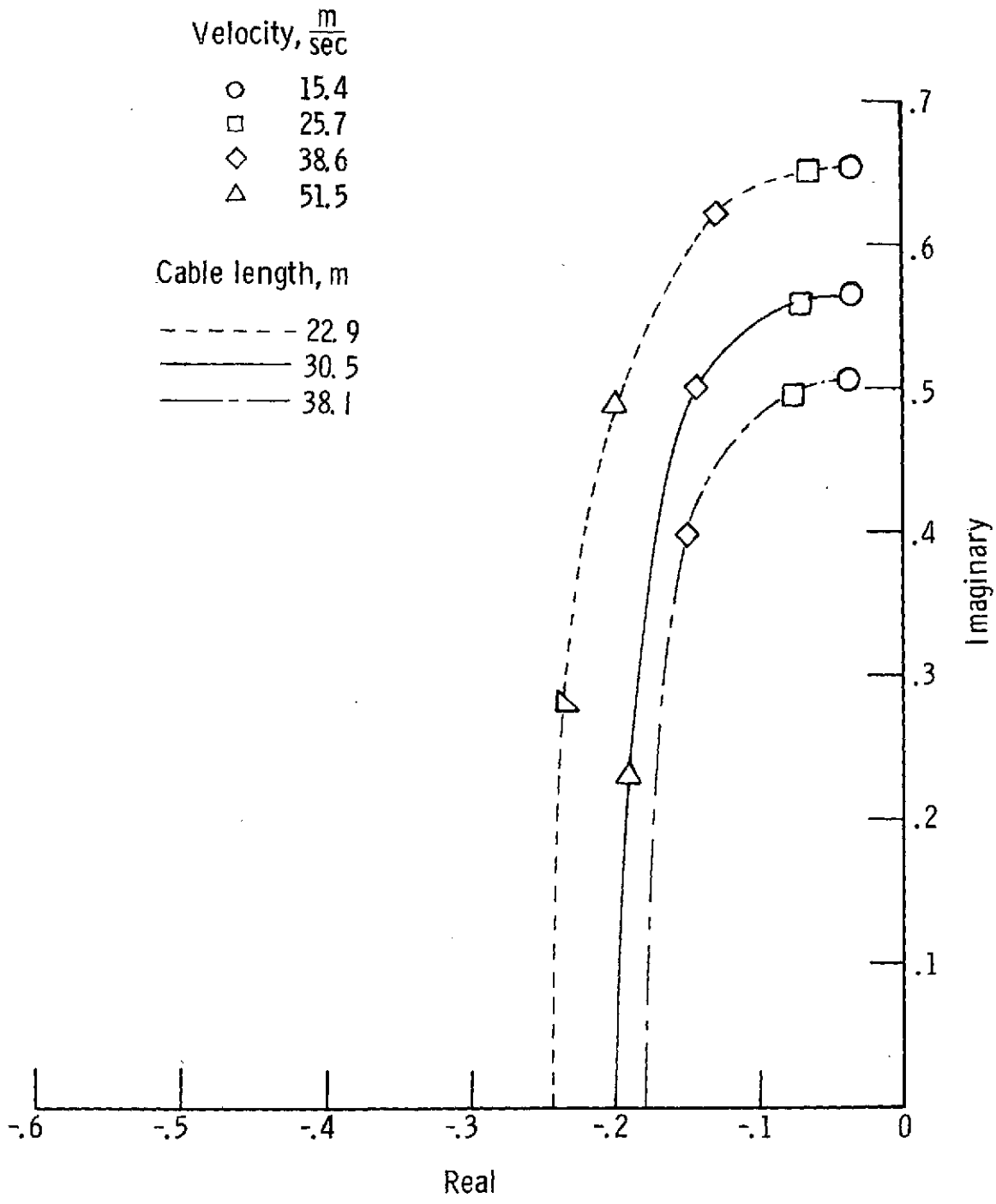

(a) Cable length.

Figure 2.- Effects of changing cable length, load mass, radius of gyration, and atmospheric density on the pendulous motion at various towing speeds.

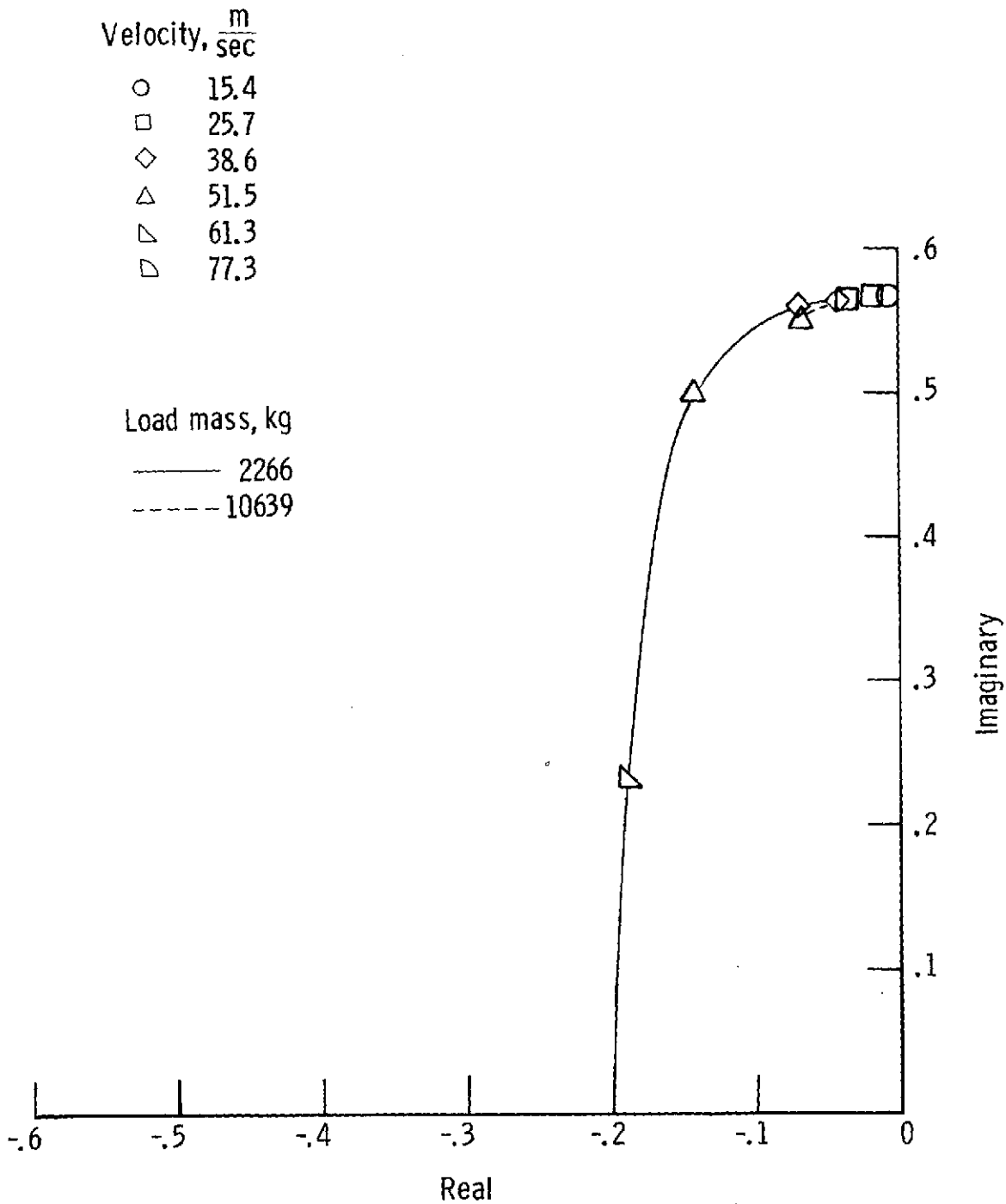

(b) Load mass.

Figure 2.- Continued.

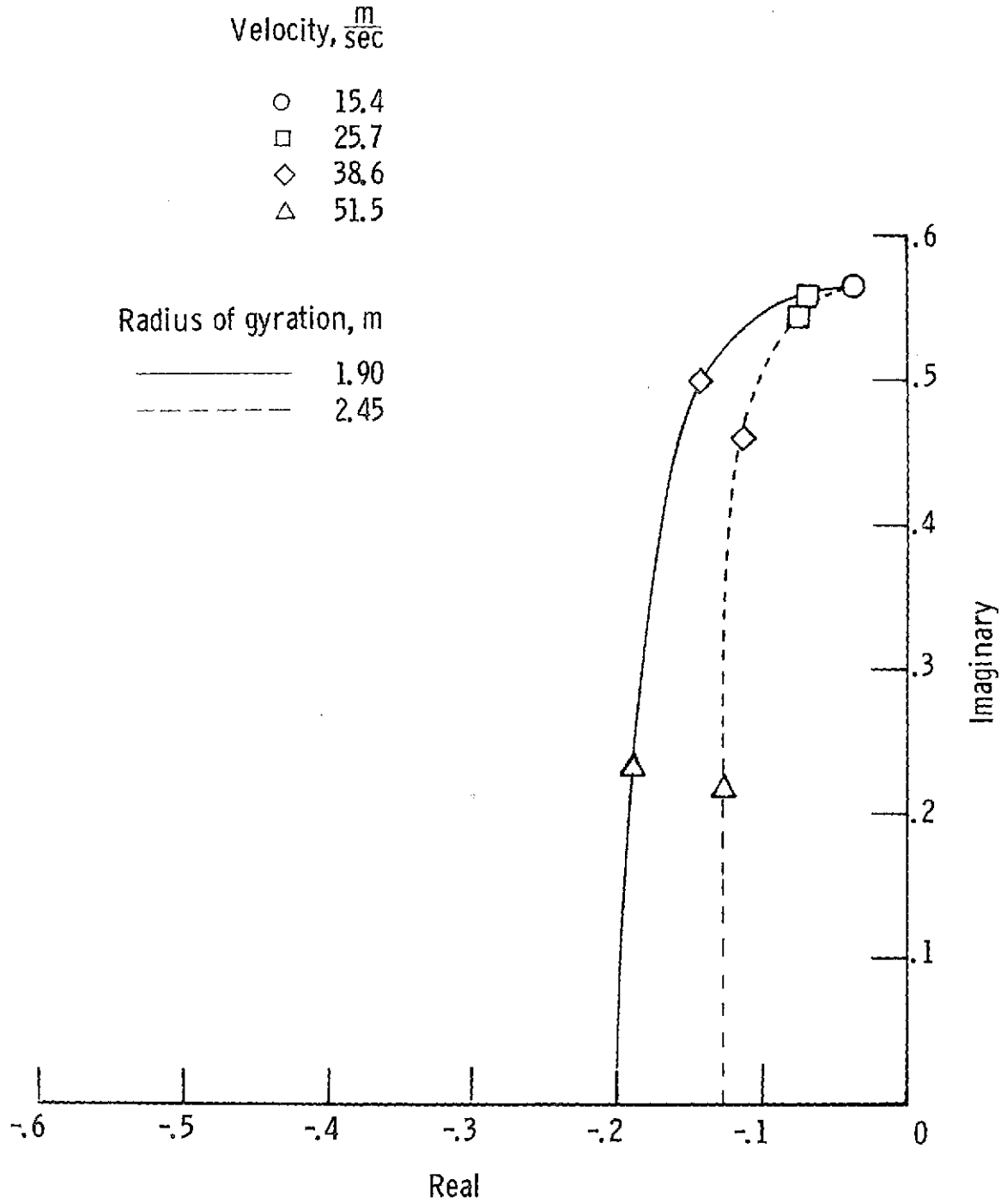

(c) Radius of gyration.

Figure 2.- Continued.

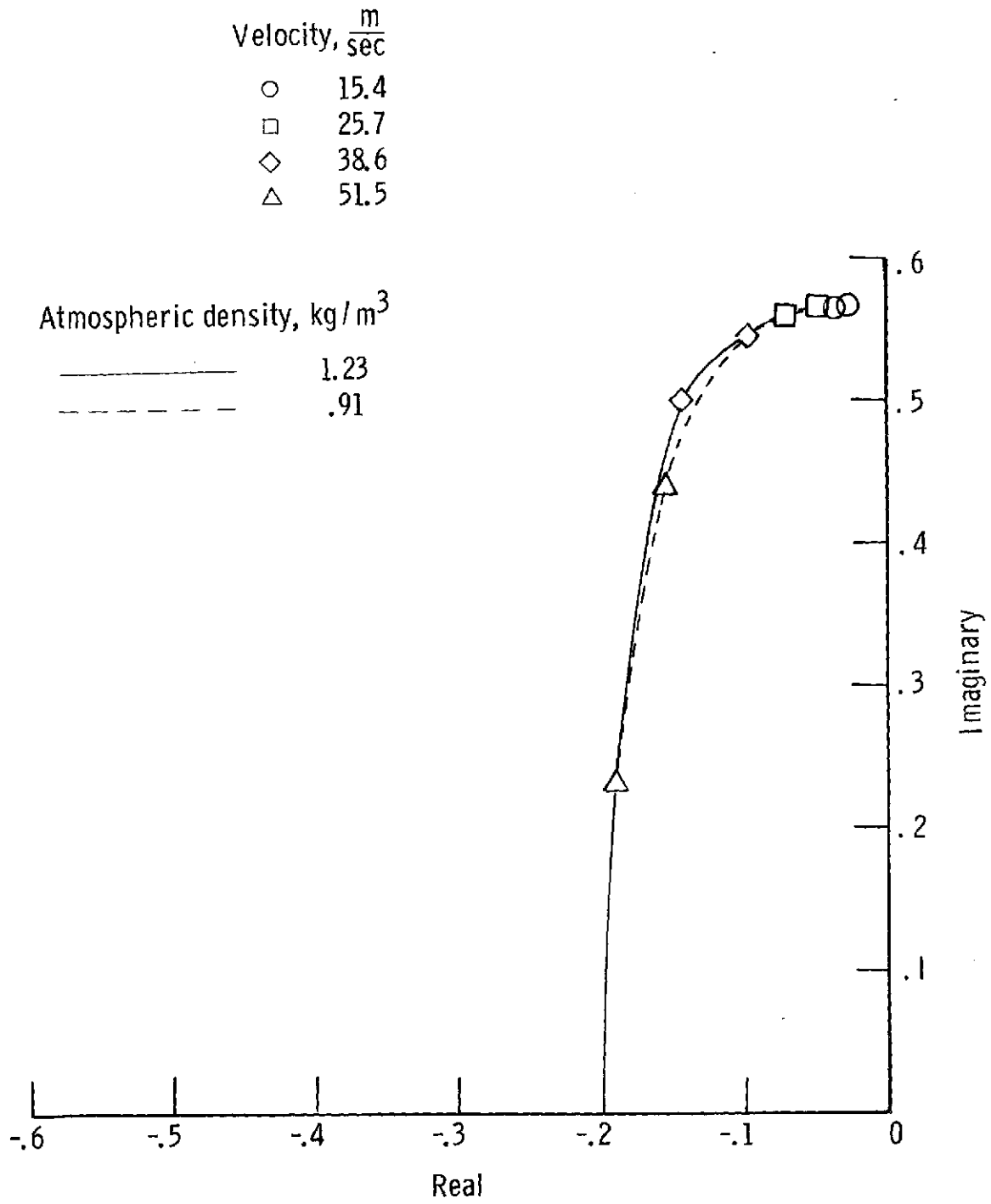

(d) Atmospheric density.

Figure 2.- Concluded.

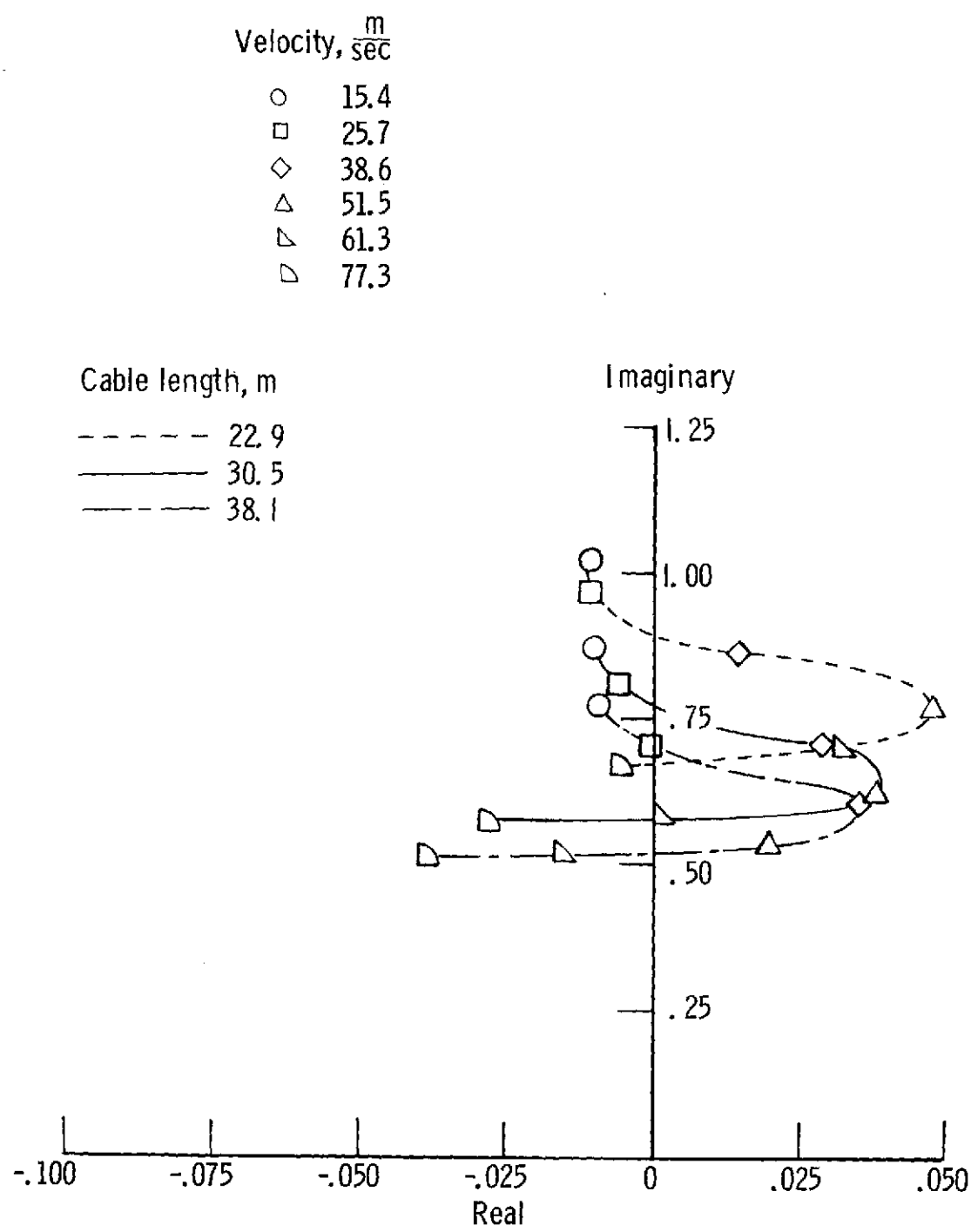

(a) Cable length.

Figure 3.- Effects of changing cable length, load mass, radius of gyration, and atmospheric density on the yawing motion at various towing speeds.

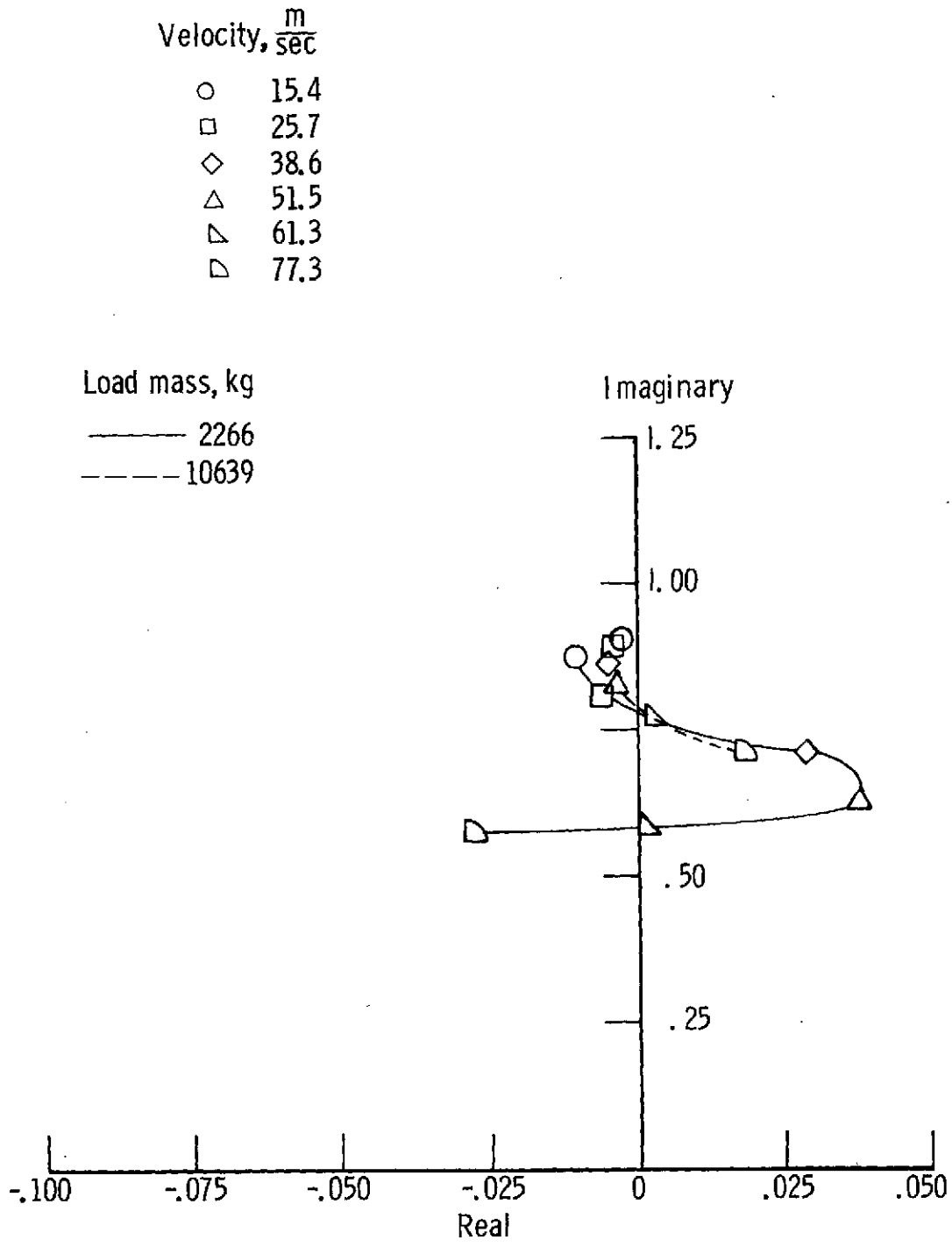

(b) Load mass.

Figure 3.- Continued.

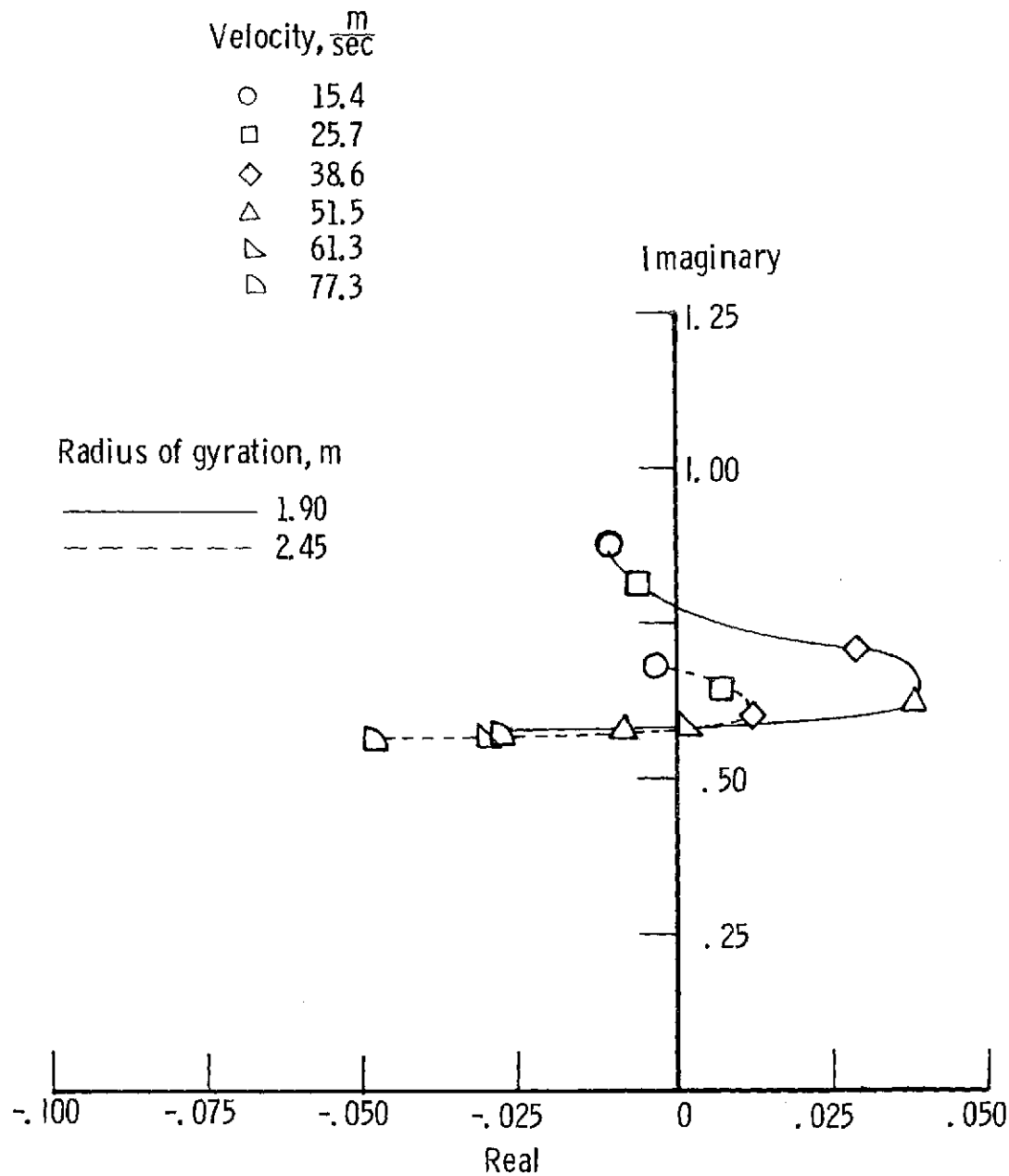

(c) Radius of gyration.

Figure 3.- Continued.

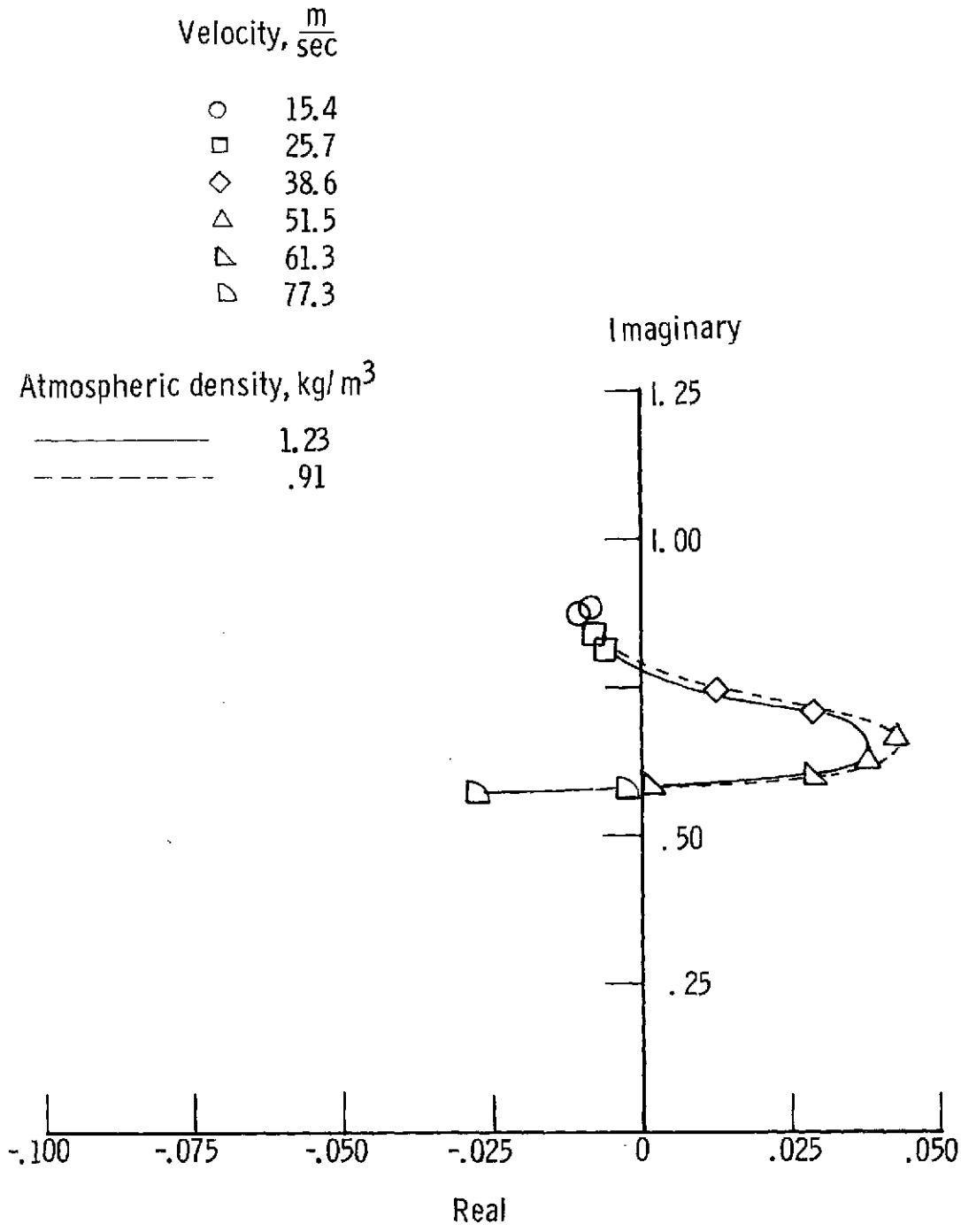

(d) Atmospheric density.

Figure 3.- Concluded.

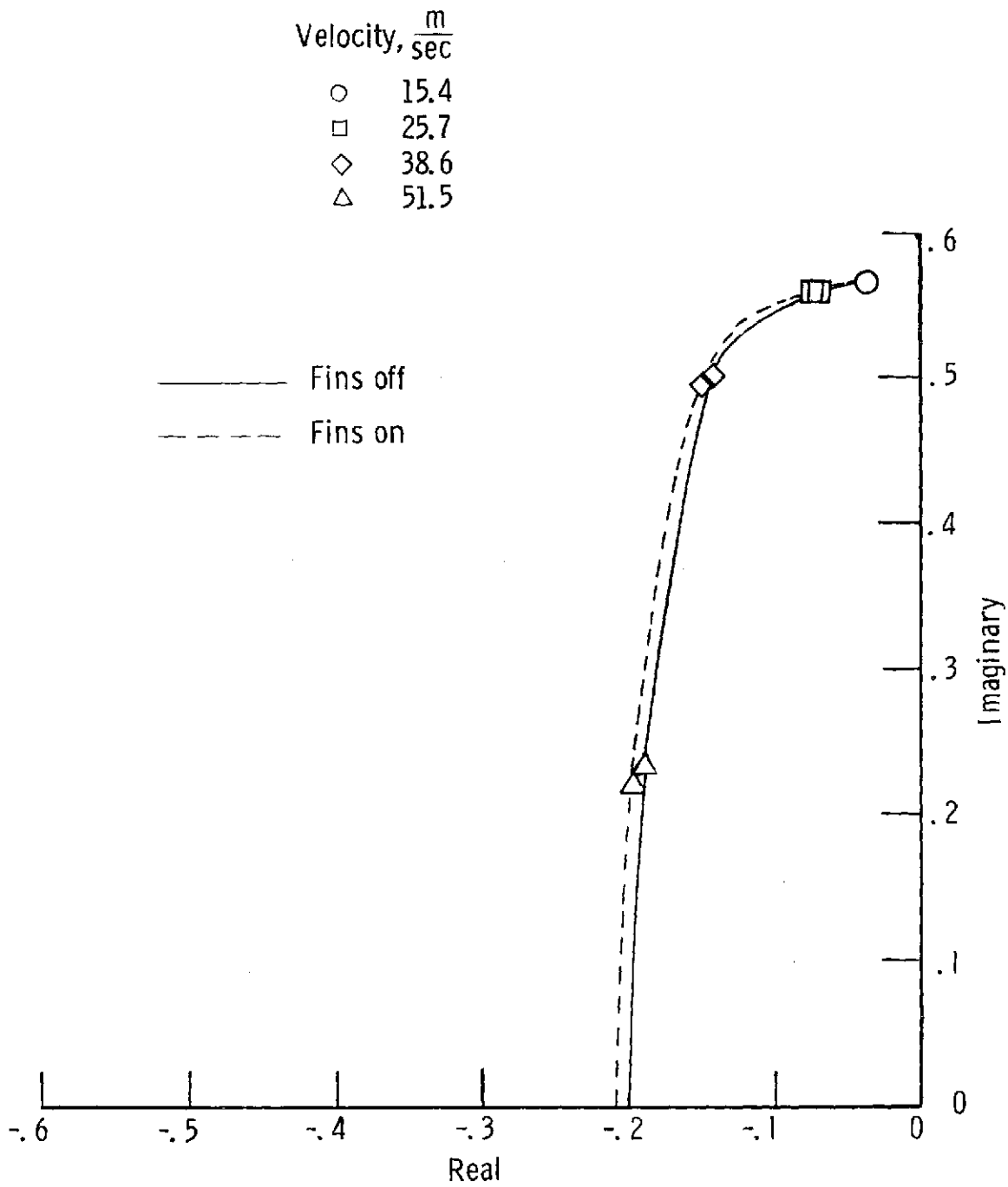

(a) Pendulous motion.

Figure 4.- Effect of stationary fins on pendulous and yawing motions at various towing speeds.

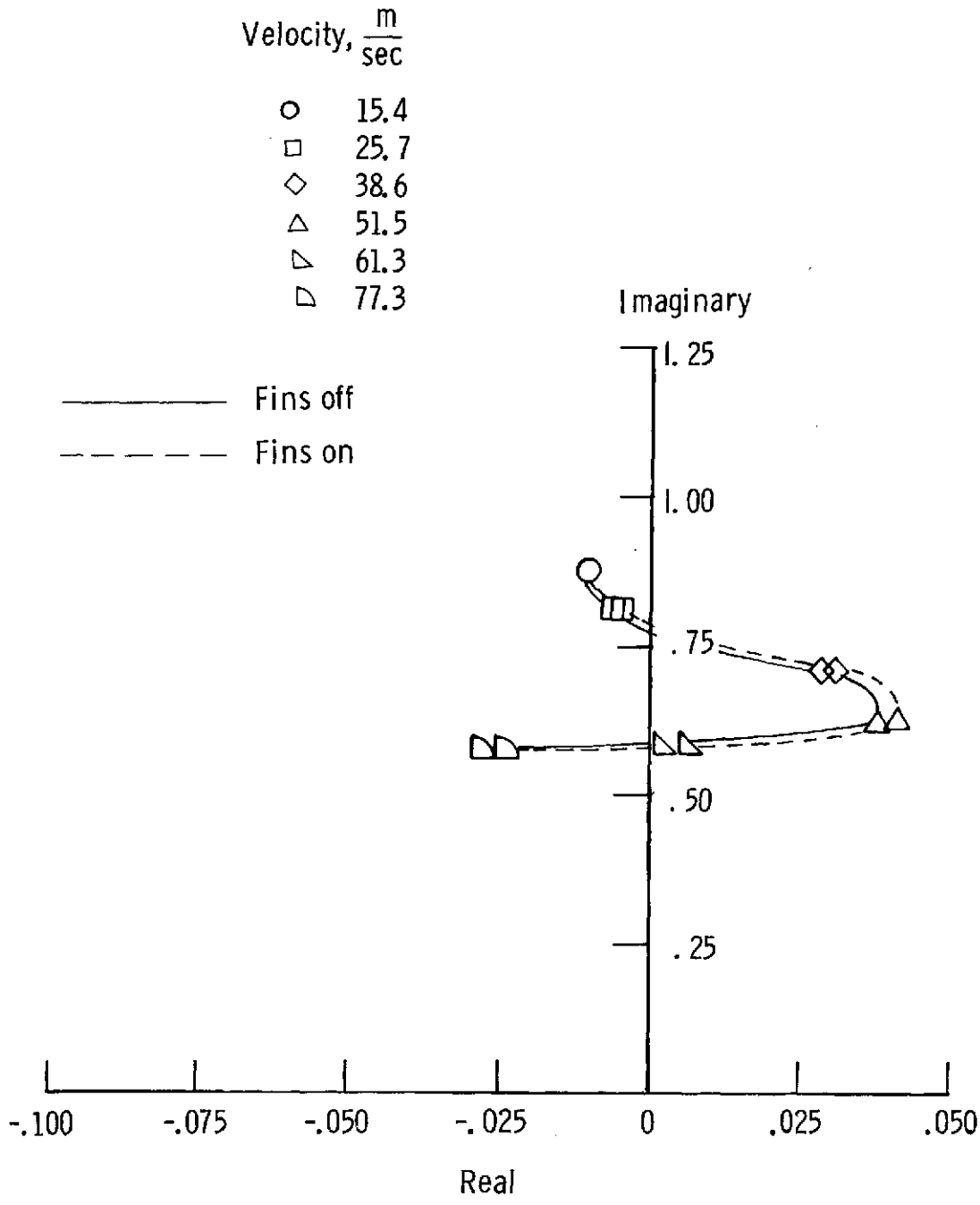

(b) Yawing motion.

Figure 4.- Concluded.

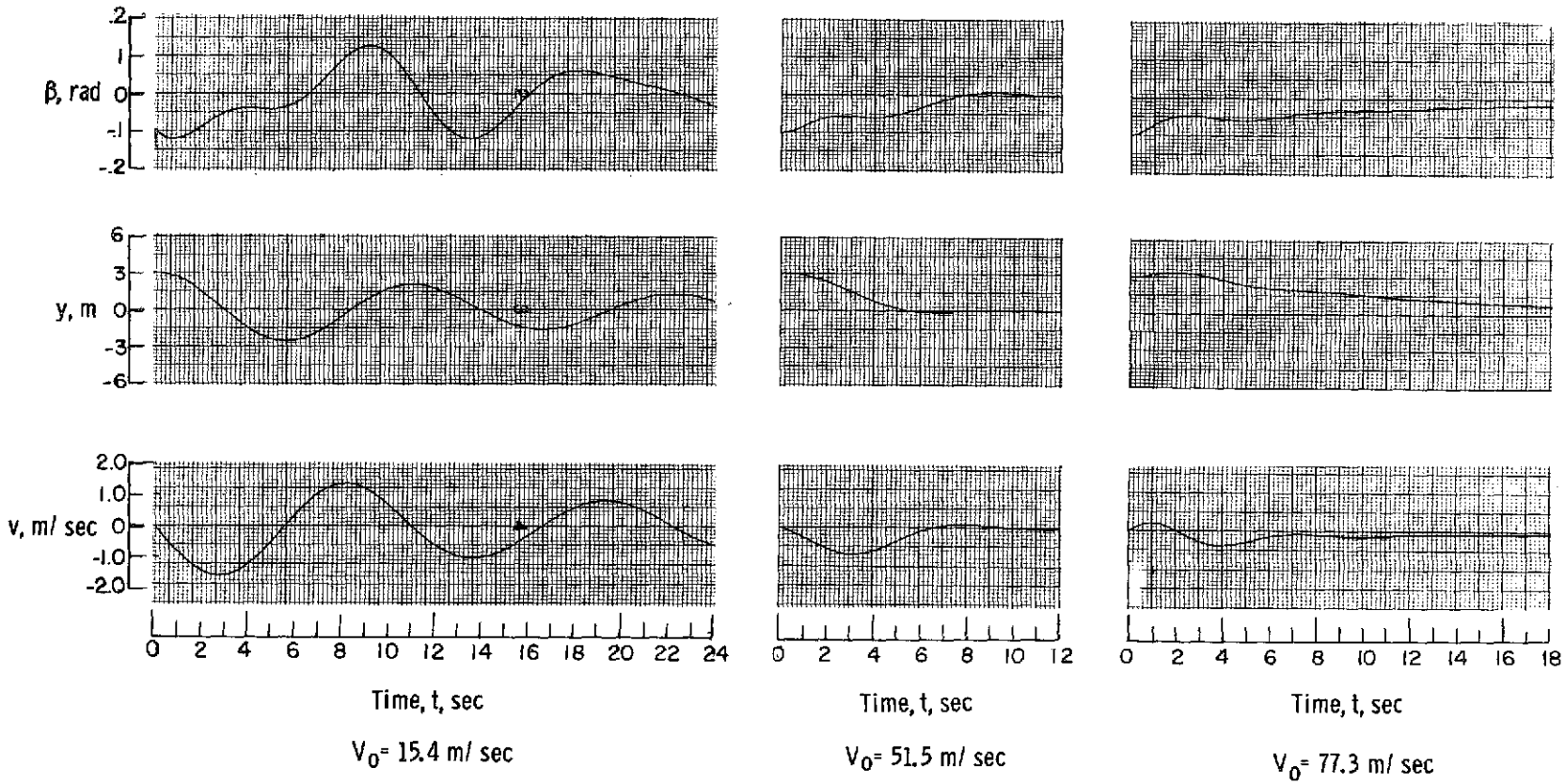

(a) β, y, and v.

Figure 5.- Closed-loop behavior of container at various towing speeds.

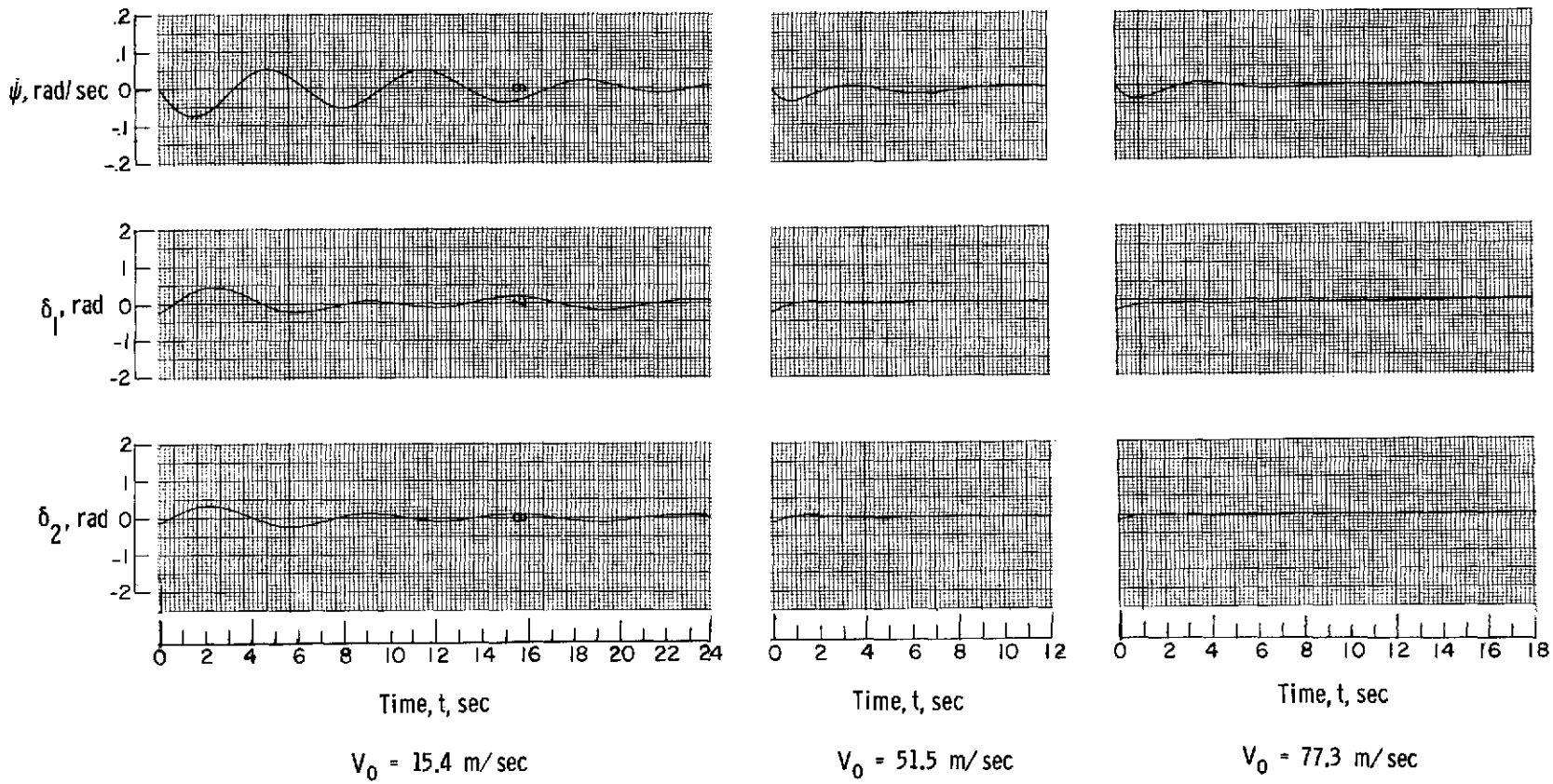

(b) $\dot{\psi}$, δ_1, and δ_2.

Figure 5.- Concluded.

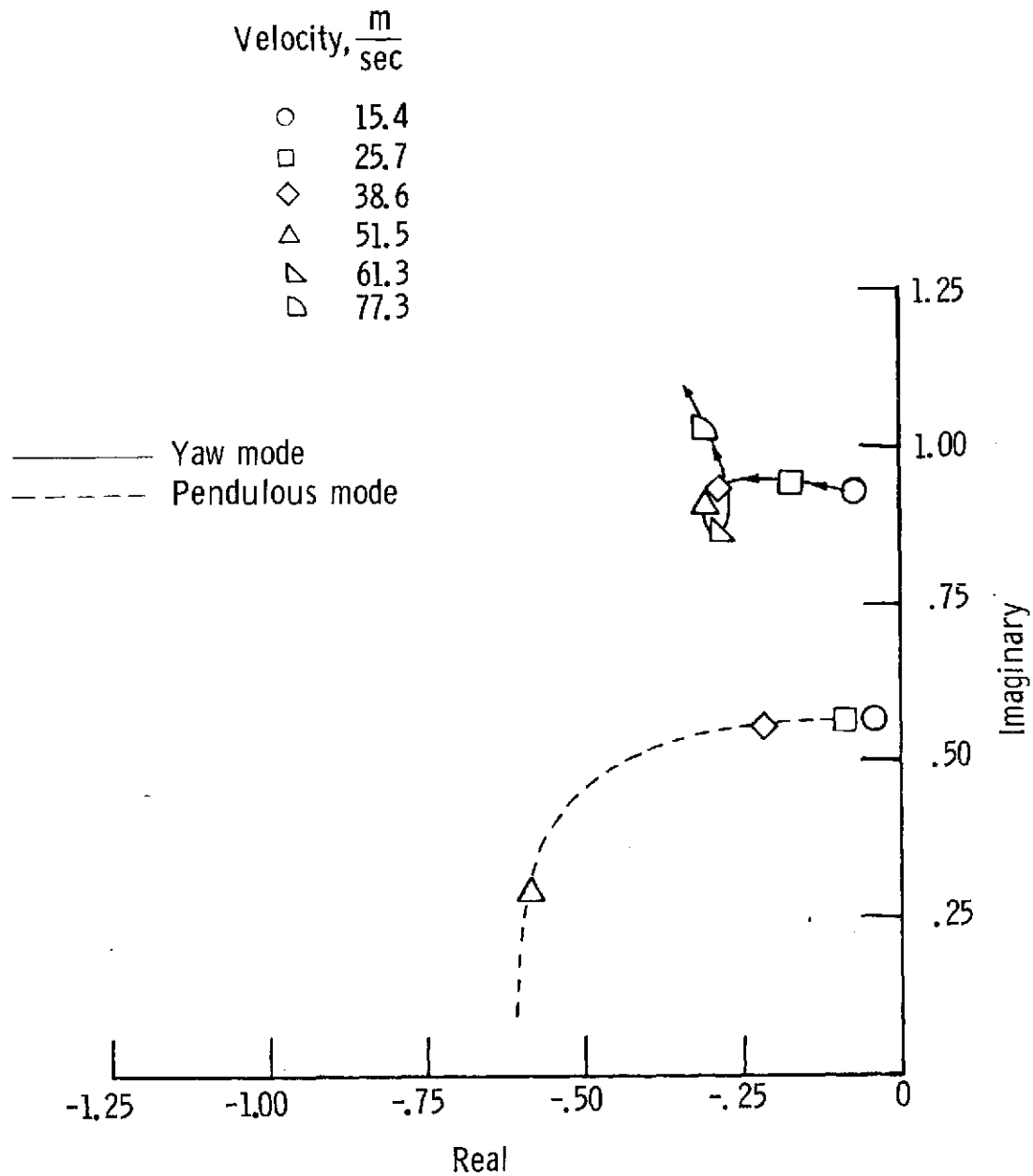

Figure 6.- Closed-loop behavior of the characteristic values associated with yawing and pendulous motions as a function of towing speed.

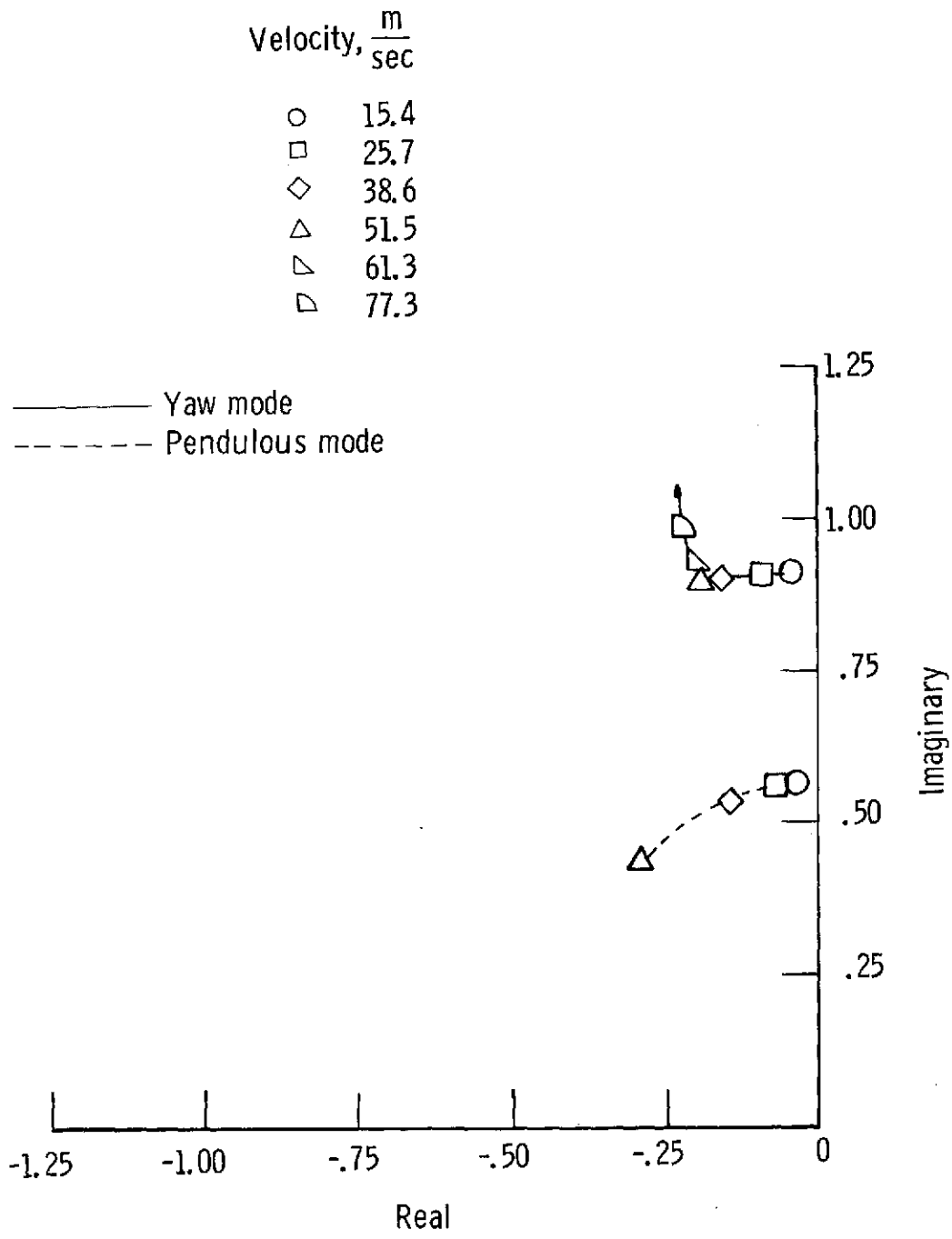

(a) Front fin failed.

Figure 7.- Effects of fin failure on yawing and pendulous motions at various towing speeds.

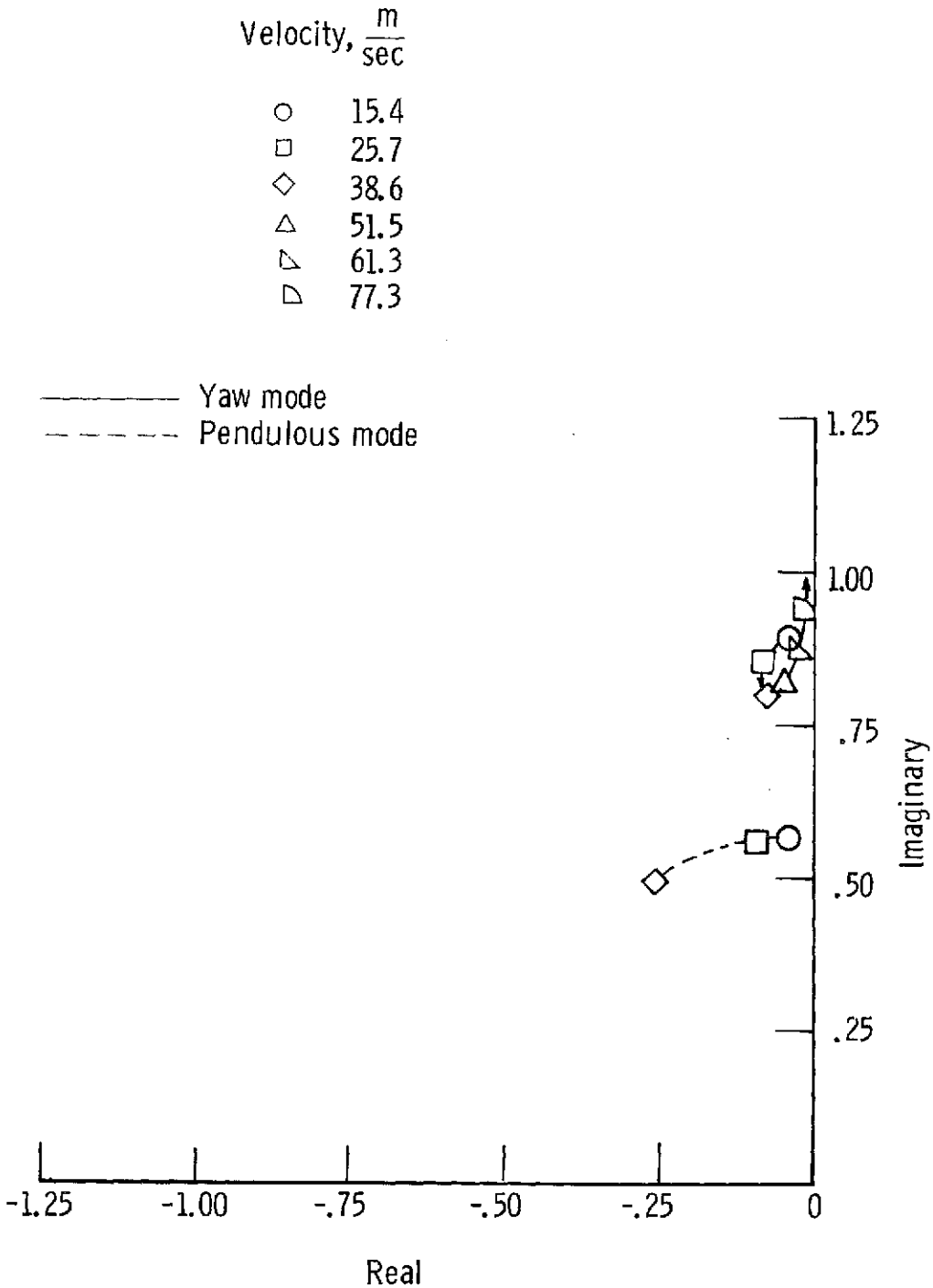

(b) Rear fin failed.

Figure 7.- Concluded.

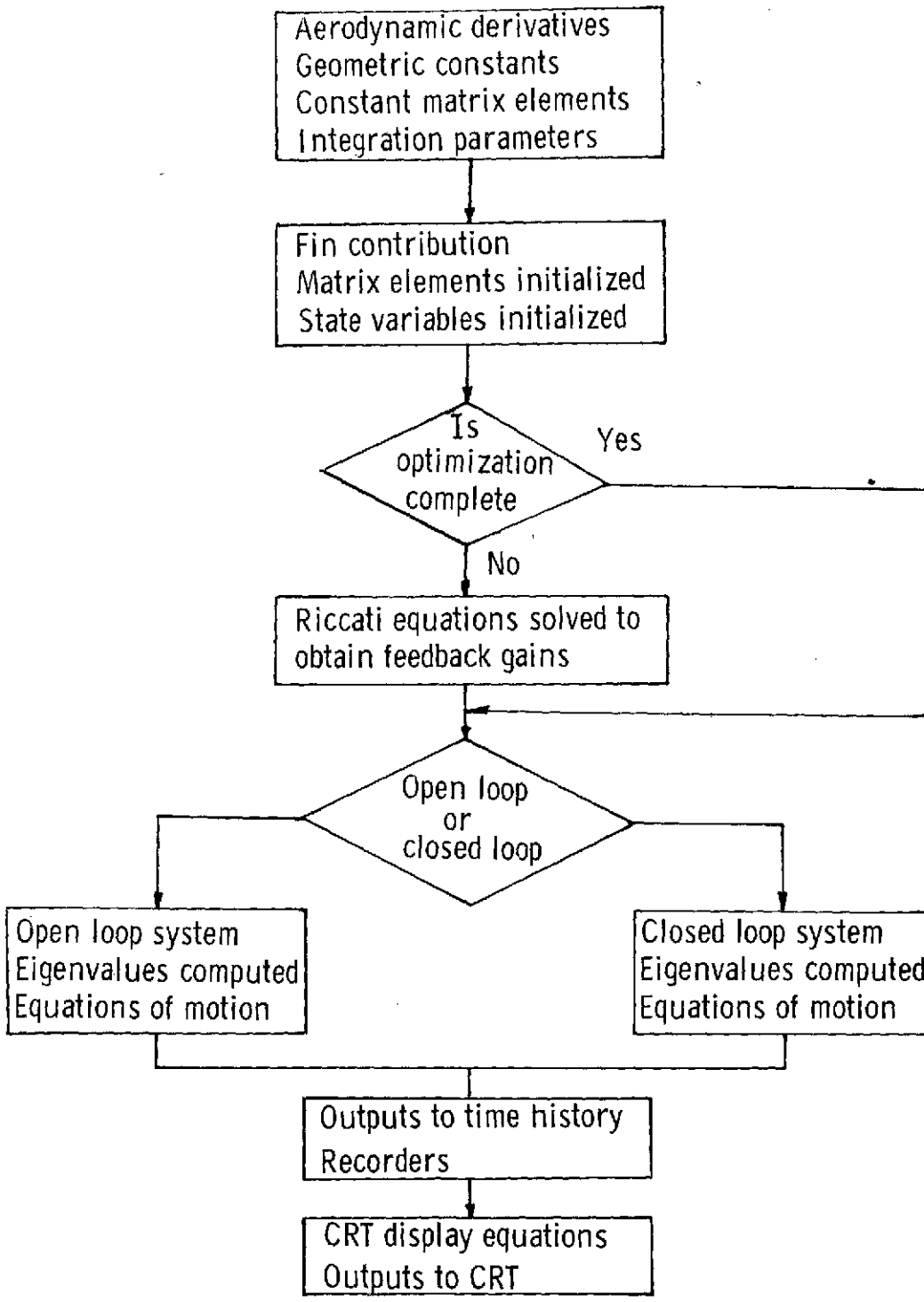

Figure 8.- Functional block flow diagram.

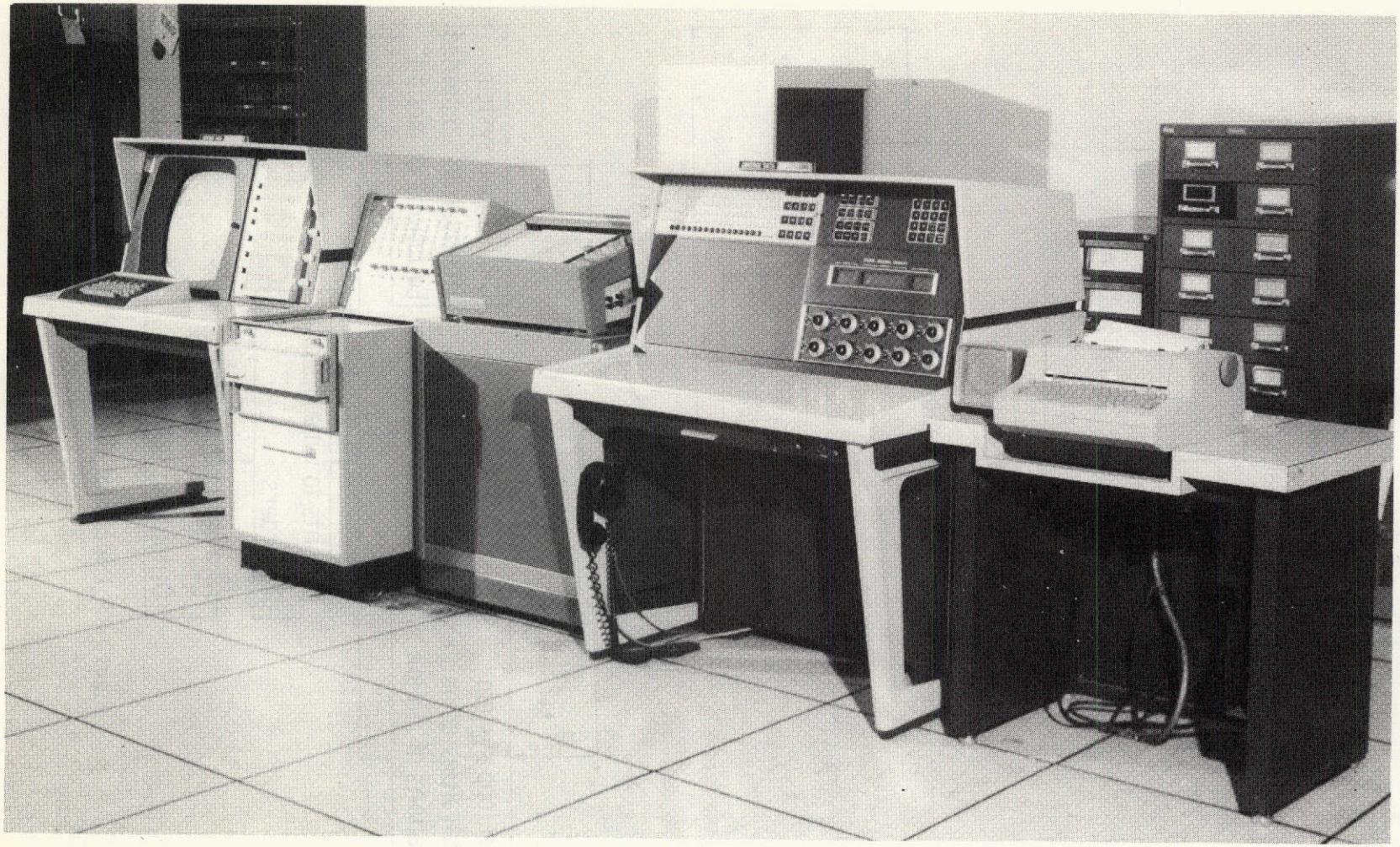

L-69-8762

Figure 9.- Typical program control station.